



**SYNTHESIS AND STRUCTURE MODIFICATION OF TITANIA
NANOTUBES FOR ENERGY CONVERSION**



RINNATHA VONGWATTHAPORN

**A THESIS SUBMITTED IN PARTIAL FULFILLMENT OF THE
REQUIREMENTS FOR THE DEGREE OF DOCTOR OF PHILOSOPHY**

MAJOR IN PHYSICS

FACULTY OF SCIENCE

UBON RATCHATHANI UNIVERSITY

ACADEMIC YEAR 2016

COPYRIGHT OF UBON RATCHATHANI UNIVERSITY



UBON RATCHATHANI UNIVERSITY
THESIS APPROVAL
DOCTOR OF PHILOSOPHY
IN PHYSICS FACULTY OF SCIENCE

TITLE SYNTHESIS AND STRUCTURE MODIFICATION OF TITANIA
NANOTUBES FOR ENERGY CONVERSION

AUTHOR MRS. RINNATHA VONGWATTHAPORN

EXAMINATION COMMITTEE

ASST. PROF.DR. TOSAWAT SEETAWAN	CHAIRPERSON
ASST. PROF. DR. UDOM TIPPARACH	MEMBER
ASSOC. PROF. DR. SUPAKORN PUKIRD	MEMBER

ADVISOR

Udom Tipparach

.....
(ASST. PROF. DR. UDOM TIPPARACH)

Utith Inprasit

.....
(ASSOC. PROF. DR. UTITH INPRASIT)
DEAN, FACULTY OF SCIENCE

Ariyaporn Pongrat

.....
(ASSOC. PROF. DR. ARIYAPORN PONGRAT)
VICE PRESIDENT
FOR ACADEMIC AFFAIRS

COPYRIGHT OF UBON RATCHATHANI UNIVERSITY

ACADEMIC YEAR 2016

ACKNOWLEDGEMENTS

I thank my advisor, Asst. Prof. Dr. Udom Tipparach, who have helped me in many respects, encouraged, guided and supported from the initial to the final level that enable me to develop understanding physical and real worlds. Special thanks the also to Assoc. Prof. Supakorn Pukird, Department of Physics, Ubon Ratchathani University for him brings me experience research lab at South Korea and helpful suggestions.

I am indebted to Dr. Greg Heness, Department of Physics and Advanced Materials, University of Technology Sydney, Australia, who gave useful suggestion, taught about sample preparation and characterization, and provided valuable information.

I appreciate the thesis committee; Assoc. Prof. Dr. Tosawat Seetawan and Assoc. Prof. Dr. Supakorn Pukird for their kindly advices and helpful suggestions. I would like to thank the external committee member, Assoc. Prof. Dr. Tosawat Seetawan and Assoc. Prof. Dr. Supakorn Pukird teaching and technical supports for this work.

Most of all, I thank my beloved family for their encouragement supports and nourishment that found me to be a fortitude person.

รินนัทธนา วังวาทธปORN

Rinnatha Vongwatthaporn

Researcher

บทคัดย่อ

ชื่อเรื่อง : การสังเคราะห์และการปรับปรุงโครงสร้างของท่อนาโนไททาเนียเพื่อการผันพลังงาน
ผู้วิจัย : รินทรนฐา วงศ์วัตถาภรณ์
ชื่อปริญญา : ปรัชญาดุขฎิบัณฑิต
สาขาวิชา : ฟิสิกส์
อาจารย์ปรึกษา : ผู้ช่วยศาสตราจารย์ ดร.อุดม ทิพรราช
คำสำคัญ : ท่อนาโนไททาเนีย, แอนโดเซชัน, เซลล์แสงอาทิตย์สีย้อมไวแสง, การผันพลังงาน

ท่อนาโนไททาเนีย (TNTs) บริสุทธิ์และเจือสังกะสีได้ถูกสังเคราะห์โดยวิธีแอนโดเซชัน การแอนโดเซชันได้ถูกดำเนินการภายใต้สารละลายอิเล็กโทรไลต์ที่ประกอบด้วย เอทิลีนไกลคอล (EG), แอมโมเนียม ฟลูออไรด์ (0.3 wt % NH_4F), น้ำปราศจากไอออน (2 Vol % H_2O) กับสาร เจือซิงค์ฟลูออไรด์ (ZnF_2) ด้วยความเข้มข้น 1 wt%, 2 wt%, 3 wt% เครื่องจ่ายแรงดันไฟฟ้า กระแสตรงค่าคงที่ 50 โวลต์ ถูกใช้ในกระบวนการแอนโดเซชัน ตัวอย่างที่ได้จากแอนโดซ์ถูกเผา ที่อุณหภูมิ 450 องศาเซลเซียส เป็นเวลา 2 ชั่วโมง ตัวอย่างที่ได้ถูกศึกษาลักษณะบ่งชี้ด้วยเทคนิคต่างๆ เทคนิคการเลี้ยวเบนของรังสีเอ็กซ์ (XRD) ถูกใช้เพื่อศึกษาโครงสร้างผลึก กล้องจุลทรรศน์อิเล็กตรอน แบบส่องกราด (SEM) ใช้ศึกษาลักษณะพื้นผิว เทคนิคเอ็กซ์พีเอส (XPS) ใช้ศึกษาองค์ประกอบทางเคมี ของพื้นผิว ผลการวิจัยพบว่า ท่อนาโนไททาเนีย (TNTs) มีโครงสร้างอนาเทส เส้นผ่านศูนย์กลางและความหนาของท่อนาโนไททาเนียมีไดออกไซด์โดยประมาณคือ 66 นาโนเมตร และ 15 นาโนเมตร ตามลำดับ เซลล์แสงอาทิตย์สีย้อมไวแสง (DSSCs) ที่ทำจากท่อนาโนไททาเนีย (TNTs) เจือซิงค์ฟลูออไรด์ (ZnF_2) มีประสิทธิภาพการผันพลังงานแสงไปเป็นพลังงานไฟฟ้า 4.54 % ภายใต้การส่องแสง 100 มิลลิวัตต์ต่อตารางเซนติเมตร (mW/cm^2) เมื่อเจือด้วยซิงค์ฟลูออไรด์ (ZnF_2) ความเข้มข้น 1 wt%

ABSTRACT

TITLE : SYNTHESIS AND STRUCTURE MODIFICATION OF TITANIA
NANOTUBES FOR ENERGY CONVERSION
AUTHOR : RINNATHA VONGWATTHAPORN
DEGREE : DOCTORAL OF PHILOSOPHY
MAJOR : PHYSICS
ADVISOR : ASST. PROF. UDOM TIPPARACH, Ph.D.
KEYWORDS : TITANIA NANOTUBE, ANODIZATION, DYE SENSITIZED
SOLAR CELLS, CONVERSION

Pure and zinc (Zn)-doped titania nanotubes (TNTs) were fabricated by means of the anodization method which was carried out in a mixture of electrolytes prepared by combining ethylene glycol (EG), ammonium fluoride (0.3 wt % NH_4F), and de-ionized water (2 Vol % H_2O) with 1 wt%, 2 wt%, and 3 wt% concentrations of dopant zinc fluoride (ZnF_2). A constant dc power supply of 50 V was used as anodic voltage. Anodized samples were annealed at 450 °C for 2 hours. The resultant samples were characterized by several techniques, x-ray diffraction (XRD) for structure and phase analysis, scanning electron microscopy (SEM) for surface morphology, and x-ray photoelectron spectroscopy (XPS) for chemical composition analysis. The results showed that the diameters and thicknesses of titanium dioxide (TiO_2) NTs were about 66 nm and 15 nm respectively. The efficiency of the dye-sensitized solar cells made from Zn-doped TiO_2 NTs was 4.54% under illumination of 100 mW/cm^2 when 1 wt% of ZnF_2 dopant was used.

CONTENT

	PAGE
ACKNOWLEDGMENT	I
THAI ABSTRACT	II
ENGLISH ABSTRACT	III
CONTENTS	IV
LIST OF TABLES	VI
LIST OF FIGURES	VII
CHAPTER 1 INTRODUCTION	
1.1 Introduction	1
1.2 Objectives	3
1.3 Scope of research	3
1.4 Expected outcomes	3
1.5 Research methods	4
CHAPTER 2 REVIEW OF LITERATURES	
2.1 Renewable energy	5
2.2 Solar energy	8
2.3 Introduction of TiO ₂	10
2.4 Nanostructures material	14
2.5 Mechanism of Titania Nanotube arrays formation by anodization method	17
2.6 Fabrication of TiO ₂ Nanotube Arrays by Electrochemical Anodization	19
2.7 Factors Affecting Utilizing TiO ₂ Nanotube Arrays	25
2.8 Doping Titania Nanotube arrays	30
2.9 Zinc incorporation of Titania Nanostructures	34
2.10 Dye sensitized solar cells (DSSCs)	36
CHAPTER 3 EXPERIMENTAL PROCEDURES	
3.1 Materials and nanotubes preparation	41
3.2 Preparation of ZnF ₂ doped TiO ₂ nanotubes	42

CONTENT (CONTINUED)

	PAGE
3.3 Characterization Techniques of ZnF ₂ doped TiO ₂ nanotubes	43
3.4 Fabrication and testing of a DSSCs	47
CHAPTER 4 RESULTS AND DISCUSSION	
4.1 Preparation and modification of Titania Nanotube arrays by anodization method	49
4.2 Characterization of TiO ₂ Nanotubes	50
4.3 XRD Analysis	52
4.4 XPS patterns	53
4.5 The efficiencies of dye-sensitized solar cells	55
CHAPTER 5 CONCLUSION AND RECOMMENTDATIONS	57
REFERENCES	59
CURRICULUM VITAE	71

LIST OF TABLES

TABLE		PAGE
2.1	Basic properties of three crystal structures of TiO ₂	11
4.1	Efficiencies of DSSCs with ZnF ₂ -doped TNT with different amounts of ZnF ₂	56

LIST OF FIGURES

FIGURE		PAGE
2.1	Preparation process of TiO ₂ nanotube by template method	12
2.2	Schematic diagram for the formation of TiO ₂ nanotubes by hydrothermal method	13
2.3	The schematic set-up for anodic oxidation method	14
2.4	Types of nanocrystalline materials by size of their structural elements: 0D (zero-dimensional) clusters; 1D (one-dimensional) nanotubes, fibers and rods; 2D (two-dimensional) films and coats; 3D (three-dimensional) polycrystals.	15
2.5	The formation of tubular structures	19
2.6	Typical current-time characteristics and corresponding growth stages during anodization process	21
2.7	Solar energy spectrum for an air mass (AM) of 1.5 in terms of the number of photons as a function of photon energy, showing different photon flux regimes available for the conversion of solar energy (area under curve); band gap of commonly available TiO ₂ and effect of band gap reduction through appropriate processing are also shown	31
2.8	A schematic of the preparation process for Zn doped TNTA	35
2.9	Schematic representation of the dye-sensitized solar cell	37
2.10	Operation principles and energy levels of nanocrystalline DSSCs	37
3.1	Flowchart of preparation of ZnF ₂ doped TiO ₂ nanotubes by anodization method for dye sensitized solar cells	40
3.2	DC Anodization apparatus	41
3.3	DC Anodization method and samples	42
3.4	AJEOL JSM-6010LV Scanning Electron Microscopy	43
3.5	Philips X'Pert-MDP X-ray diffractometer	44
3.6	Schematic diagram of X-ray Diffractometer	45
3.7	Bragg's law and diffraction through crystal planes	45
3.8	Thermo Al K- Alpha XPS machine (South Korea)	46

LIST OF FIGURES

FIGURE		PAGE
3.9	Shows measurement device of J-V curves for DSSCs	47
3.10	J-V curves for dye-sensitized solar cells	48
4.1	The Ti sheets were cut in circular shape with diameter of 1.4 cm	49
4.2	SEM images of TiO ₂ nanotube arrays with different doped ZnF ₂ : Undoped (b) Doped 1.0 wt% of ZnF ₂ (c) Doped 2.0 wt% of ZnF ₂ and (d) Doped 3.0 wt% of ZnF ₂	50
4.3	XRD patterns of TiO ₂ nanotube arrays with ZnF ₂	52
4.4	XPS spectra of ZnF ₂ doped TiO ₂ nanotubes with different doped ZnF ₂ : Undoped (b) Doped 1.0 wt%, of ZnF ₂ (c) Doped 2.0 wt% of ZnF ₂ and (d) Doped 3.0 wt% of ZnF ₂	53
4.5	Current-Voltage curves of DSSCs with TNT doped with different amounts of ZnF ₂ using ammonia as source - (a) undoped, (b) 1.0 wt%, (c) 2.0 wt%, and (d) 3.0 wt%	56

CHAPTER 1

INTRODUCTION

1.1 Introduction

Global energy crisis such as high oil price and energy shortage due to growing population and expanding industrialization, and exhaustion of natural energy sources such as fossil fuels, coal, oil and natural gas, has triggered the need for developing alternative sources of energy that are renewable, clean and low cost. In addition, the use of energy especially fossil fuels causes air pollution due to emission of greenhouse gases. Solar energy is an excellent energy source because it's natural, abundant and inexhaustible. Solar cells and other photovoltaic devices are being used to harness energy from the sun. The invention of the dye-sensitized solar cells (DSSCs) by Gratzel and O'Regan in 1991 [1] has led to intensive research to improve solar cell efficiency.

TiO₂ semiconductor has been extensively studied in recent years due to its high photocatalytic activity, dielectric effect, resistance to corrosion, nontoxicity, and low cost. These unique properties make it a suitable material for several applications such as in photocatalysis [1], humidity sensing [2], water splitting [3], hydrogen generation [4], and gas sensing [5].

The use of TiO₂ means its solar energy absorption is restricted mostly in the ultraviolet region due to its large energy band gap (3.2 eV for anatase). In addition, high rate of charge recombination limits its practical applications. These problems can be solved by modifying the structure of titania through doping with foreign ions [6, 7] or through developing nanotubes of TiO₂ [8, 9].

TiO₂ nanotubes have been successfully fabricated using techniques such as hydrothermal [10], solvothermal [11], sol-gel [12] and anodization [13-15] methods. Of these methods, anodization is a more suitable method due to its simplicity and low cost. Several parameters have been investigated in the preparation and application of titania nanotubes. These include: electrolyte composition, electrolyte pH, anodization time, anodizing voltage, dopant element and annealing temperature [16 -21].

Anodization is an electrolytic process that creates a protective oxide film over a metallic surface. Anodization of titanium foil was carried out in two-electrode electrochemical cells at constant applied voltage. The use of different electrolyte solutions permits control of the architecture from well separation an open top and bottom closed by barrier layer of metal [22]. Fabrication of titania nanotube arrays by anodic oxidation in electrolyte containing fluoride possess many excellent properties such as highly ordered, uniform diameter and length [23]. There are many effects on the growth of titania nanotubes including the anodization voltage and current density, anodization time, fluoride concentration, pH of electrolyte, and preparation of electrolyte [23–26]. All these parameter could influence the efficiency of their photocatalytic activity. Furthermore, doped titania nanotube arrays have been extensively investigated due to their capability to narrow band gap and extend the wavelength response of TiO_2 nanotube arrays into the visible light region and inhibits phase transformation [27]. Many researchers have recently paid their attention on studying new techniques for preparing titania nanotube arrays. Various studies have been interested to improve photocatalytic efficiency of titania nanotube arrays.

Most titania catalysts require activation by ultraviolet light which comprises only about 4% of the solar energy spectrum [22]. To improve the photocatalytic reactivity of TiO_2 and to extend its light absorption into the visible region several methods have been considered such as controlling band gap energy (3.2 eV in the anatase TiO_2 crystalline phase) through doping nonmetal materials and enlarging the surface area by producing titania in the form of nanoparticles, nanowires and nanotubes [28–29]. In previous work, The almost common knowledge that the electrolyte needs an aging process before it can be used for an anodization fabrication of titania nanotubes which helps to synthesize well defined nanotubes [30–31] and doping with foreign elements such as Carbon (C), Nitrogen (N), Fluorine (F), Sulfur (S), Boron (B), Iodene (I) and Phosphorus (P) [22,32]. However, no detailed study has been reported on preparation and compound properties of titania synthesized by stirring the electrolyte in preparation process of solution and adding zinc fluoride in the electrolyte. So, this research proposed to prepare and investigate the nanostructure properties of undoped and ZnF_2 -doped titania nanotubes by stirring and aging of the electrolytes in preparation process in the electrolyte solutions for the electrochemical anodic

oxidation of pure titanium sheets in the mixtures of ethylene glycol, ammonium fluoride and deionized water electrolyte solution added with different zinc fluoride doping concentrations.

1.2 Objectives

1.2.1 To prepare and modify the structure of undoped and ZnF₂-doped titania nanotubes by anodization method with pure titanium sheets.

1.2.2 To investigate the microstructure and properties of undoped and ZnF₂-doped titania nanotubes by XRD, SEM images for surface morphology, X-ray photoelectron spectroscopy (XPS) chemical composition of the prepared samples.

1.2.3 To fabricate and test the efficiency of the dye sensitized solar cells (DSSCs).

1.3 Scope of research

The scope of this research is to prepare and to investigate the microstructure and the properties of undoped and ZnF₂-doped TiO₂ nanotubes by anodization method of pure titanium sheets in the mixture electrolyte, mixtures of ethylene glycol, ammonium fluoride and deionized water electrolyte solution containing with different ZnF₂ doping concentrations. The dopants were varied from 1.0 wt%, 2.0 wt% and 3.0 wt% of ZnF₂. The anodizing voltage will be set at 50 V and the process will be conducted for 2 hours. The titanium foils were anodized at room temperature. Then, the samples were subjected to mild ultrasonic treatment in ethanol for 10 min. The nanotubes were crystallized by the annealing at 450 °C for 2 hours. The titanium nanotubes will be characterized by XRD for microstructure, SEM images for surface morphology and XPS for chemical composition properties and performance test of the dye sensitized solar cells in the illuminance of 100 mW/cm².

1.4 Expected outcomes

1.4.1 Understanding the fabrication procedure for titania nanotube arrays by anodization method

1.4.2 Obtain the working electrodes for the dye sensitized solar cells for ZnF₂ doped titania nanotube.

1.5 Research methods

The titania nanotubes will be prepared by anodization methods of pure titanium sheets. The titanium sheets, 0.25 mm in thickness and more than 99.7% in purity, from Sigma Aldrich. The titanium sheets will be cut in circular shape with diameter about 1.5 cm. Before anodization, the titanium substrates will be degreased ultrasonically in turn in isopropanol, de-ionized water and ethanol [5] for 10 min. The substrates will be bound to an electrolytic cell via an o-ring and a copper (Cu) plate. One side of the substrate will be in contact with the electrolyte and the opposite side, covered by a Cu plate, will be connected to the DC power supply with a conducting wire. The counter electrode will be a piece of platinum (Pt) sheet. The spacing between the two electrodes was approximately 2 cm. The electrolyte will be the mixture of ethylene glycol (EG) ammonium fluoride (0.3 wt% NH_4F), de-ionized water (2 Vol% H_2O) and containing with different concentrations of Zinc Fluoride (ZnF_2). The anodizing voltage will be set at 50V and the process will be carried out for 2 hours. The titanium foil will be anodized at room temperature. Then, the samples will be subjected to mild ultrasonic treatment in ethanol for 10 minutes in order to clean debris that covers the surfaces of the samples. The nanotubes will be crystallized by the annealing at 450 °C for 2 hours.

The titania nanotubes will be characterized by XRD for microstructure, SEM images for surface morphology and XPS for chemical composition properties and performance test in dye sensitized solar cells.

CHAPTER 2

REVIEW OF LITERATURES

2.1 Renewable energy

Recently, the world energy is largely depended on fossil fuels. The use of fossil fuels leads to atmospheric pollution, global warming and energy shortage. This may be replaced by using sustainable and renewable energy sources [25]. Renewable energy is energy that is generated from natural processes that are continuously replenished. There are many forms of renewable energy. Most renewable energy comes either directly or indirectly from the sun. Solar energy can be used directly for heating and lighting homes and other buildings, for generating electricity, for hot water heating, solar cooling, and a variety of commercial and industrial uses. Solar energy is the direct conversion of sunlight using panels or collectors. Biomass energy is stored sunlight contained in plants. Hydrogen is high in energy, yet an engine that burns pure hydrogen produces almost no pollution. Other renewable energies that do not depend on sunlight are geothermal energy, which is a result of radioactive decay in the crust combined with the original heat of accreting the Earth, and tidal energy, which is a conversion of gravitational energy.

The sun radiates energy in forms of light and heat, which depends on the nuclear fusion power from the core of the Sun. Solar energy can be collected and converted in few different ways. Two main types of solar energy systems are in use today, which including photovoltaics, and thermal systems. Photovoltaic systems convert solar radiation to electricity by a variety of methods. The most common approach is to use solar cells, which generate an electrical current when light shines upon it. Solar Thermal Systems seek to store heat from the sun that can be used for a variety of purposes. Many different approaches can be employed here, including active systems, such as solar hot water heaters, and passive systems, in which careful engineering design results in a building that automatically stores and utilizes solar energy.

Wind power is a form of solar energy. Winds are caused by the rough heating of the atmosphere by the sun, the irregularities of the earth's surface, and rotation of the earth. Wind flow patterns are modified by the earth's region, bodies of water, and vegetative cover. This wind flow, when harvested by wind turbines, can be used to generate electricity.

Hydroelectricity is the term referring to electricity generated by hydropower. This form uses the gravitational potential of elevated water that was lifted from the oceans by sunlight. It is not strictly speaking renewable since all reservoirs eventually fill up and require very expensive excavation to become useful again. At this time, most of the available locations for hydroelectric dams are already used in the developed world.

Biomass is the term for energy from plants. Energy in this form is very commonly used throughout the world. Unfortunately the most popular is the burning of trees for cooking and warmth. This process releases copious amounts of carbon dioxide gases into the atmosphere and is a major contributor to unhealthy air in many areas. Some of the more modern forms of biomass energy are methane generation and production of alcohol for automobile fuel and fueling electric power plants.

Hydrogen is the simplest element in the universe. An atom of hydrogen consists of only one proton and one electron. It's also the most plentiful element in the universe. Despite its simplicity and abundance, hydrogen doesn't occur naturally as a gas on the Earth - it's always combined with other elements. Water is a combination of hydrogen and oxygen (H_2O). Hydrogen is also found in many organic compounds, notably the hydrocarbons that make up many of our fuels, such as gasoline, natural gas, methanol, and propane. There are several promising methods to produce hydrogen, such as solar power. Currently, most hydrogen is made this way from natural gas. An electrical current can also be used to split water into its components of oxygen and hydrogen atoms. This process is known as electrolysis. Some algae and bacteria, using sunlight as their energy source, even give off hydrogen under certain conditions.

A fuel cell combines hydrogen and oxygen to produce electricity, heat, and water. Fuel cells are often compared to batteries. Both convert the energy produced by a chemical reaction into usable electric power. However, the fuel cell will produce electricity as long as fuel (hydrogen) is supplied, never losing its charge.

Geothermal energy is the heat from the Earth. It's clean and sustainable. Resources of geothermal energy range from the shallow ground to hot water and hot rock found a few miles beneath the Earth's surface, and down even deeper to the extremely high temperatures of molten rock called magma. Geothermal electricity is electricity generated by geothermal energy. Technologies in use include dry steam power stations, flash steam power stations and binary cycle power stations. In certain areas the geothermal gradient is high enough to exploit to generate electricity. This possibility is limited to a few locations on Earth and many technical problems exist that limit its utility. Another form of geothermal energy is Earth energy, a result of the heat storage in the Earth's surface. Soil everywhere tends to stay at a relatively constant temperature, the yearly average, and can be used with heat pumps to heat a building in winter and cool a building in summer. This form of energy can lessen the need for other power to maintain comfortable temperatures in buildings, but cannot be used to produce electricity.

Tidal energy is a form of hydropower that converts the energy obtained from tides into useful forms of power, mainly electricity. Although not yet widely used, tidal power has potential for future electricity generation. Tides are more predictable than wind energy and solar power. Among sources of renewable energy, tidal power has traditionally suffered from relatively high cost and limited availability of sites with sufficiently high tidal ranges or flow velocities, thus constricting its total availability. However, many recent technological developments and improvements, both in design and turbine technology, indicate that the total availability of tidal power may be much higher than previously assumed, and that economic and environmental costs may be brought down to competitive levels.

The sun is the most important source of renewable energy available to day. The sun has provided energy for practically all living creatures on earth, through the process of photosynthesis, in which plants absorb solar radiation and convert it into stored energy for growth and development. The Scientists and engineers today seek to utilize solar radiation directly by converting it into useful heat or electricity. There is a great deal of opportunity for using these systems to improve the available technology and increase the utilization of solar energy systems. Solar energy is a smart green and clean energy opportunity to add to our overall renewable energy or sustainable energy

group to help offset the use of conventional fuels, reduce harmful emissions, and meet necessary future energy goals.

2.2 Solar energy

Solar energy is healthy energy that is produced by the Sun. Every day, the Sun radiates an enormous amount of energy. The amount of energy humans use annually, about 4.6×10^{20} joules, is delivered to Earth by the Sun in one hour. The enormous power that the Sun continuously delivers to Earth, 1.2×10^5 terawatts, dwarfs every other energy source, renewable or nonrenewable. It significantly exceeds the rate at which human civilization produces and uses energy, currently about 13 terawatts [34]. The impressive supply of solar energy is complemented by its usefulness. Solar radiation is a renewable energy resource that has been used by humanity in all ages. The solar energy could be a best option for the future world because of it is abundant in nature and freely available source of energy with no cost. Moreover, it is a promising source of energy in the world because it is not exhaustible, giving solid and increasing output efficiencies than other sources of energy [33]. The discovery of photovoltaic effect by Becquerel in 1839 and the creation of the first photovoltaic cell or solar cell in the early 1950s opened entirely new perspectives on the use of solar energy for the production of electricity. Sunlight can be converted into electricity by exciting electrons in a solar cell. It can yield chemical fuel via natural photosynthesis in green plants or artificial photosynthesis in human-engineered systems. The sunlight can produce heat for direct use or further conversion to electricity. Photovoltaic technology is a technology used to convert sunlight into electricity directly without any interface for conversion. Therefore, these devices are very simple in design and for efficient handling. In addition, they have the ability to give larger outputs from smaller inputs. Thus, they are used in various applications worldwide. But, its system is still to be improved for better outputs. Photovoltaic devices commonly use semiconductor material to induce electricity, in which silicon is commonly used. The principle of this device is to activate electrons by giving additional energy. This device works on the principle that the electrons are activated from lower energy state to higher energy state as of the energy addition from sunlight. This activation will in turn create number of holes and free electrons in the semi-conductor thus giving electricity

[33]. Since then, the evolution of solar technologies continues at an unprecedented rate. Nowadays, there exist an extremely large variety of solar technologies, and photovoltaics have been gaining an increasing market share for the last 20 years. Nevertheless, the abundance and versatility of solar energy, we use very little of it to directly power human activities. Solar electricity accounts for a minuscule 0.015% of world electricity production, and solar heat for 0.3% of global heating of space and water. Biomass produced by natural photosynthesis is by far the largest use of solar energy. Its combustion or gasification accounts for about 11% of human energy needs. Between 80% and 85% of our energy comes from fossil fuels, a product of ancient biomass stored beneath Earth's surface for up to 200 million years [34]. Fossil-fuel resources are of finite extent and are distributed unevenly beneath Earth's surface. When fossil fuels are turned into useful energy through combustion, they produce greenhouse gases and other harmful environmental pollutants. In contrast, solar photons are effectively inexhaustible and unrestricted by geopolitical boundaries. Their direct use for energy production does not threaten health or climate. The solar resource's magnitude, wide availability, flexibility, and benign effect on the environment and climate make it an appealing energy source. From a scientific and technological viewpoint, the great challenge is finding new solutions for solar energy systems to become less capital intensive and more efficient. Many research efforts are addressing these problems. Low-cost and high efficiency photovoltaic device concepts are being developed. Solar thermal technologies are reaching a mature stage of development and have the potential of becoming competitive for large energy supply. Intermittency is being addressed with extended research efforts in energy storage devices, thermal storage, and the direct production of solar fuels. All these are valuable routes for enhancing the competitiveness and performance of solar technologies.

Over the years there have been several studies on semiconductor photocatalytic and photoelectronchemical systems for hydrogen generation or water splitting reaction. The underlying operating principles have also been extended to many other areas such as electrochemical photovoltaics, wastewater treatment, antibacterial, self-cleaning, and fuel synthesis. The conversion of radiant energy to electrical or chemical energy is primarily based upon the pumping of electrons to higher energy levels upon

the absorption of light in the visible or ultra violet regions. Intermolecular electron transfer from these excited molecules, either directly or via an external circuit in an electrochemical cell, provides the basis of the energy conversion process. Generally, when a semiconductor surface is exposed to light radiation, electron hole pairs are generated. Efficient utilization of the radiant energy requires separation of the photogenerated electron-hole pairs before recombination. These events have been found to occur quite effectively within the electric field formed at the interface between a semiconductor and an electrolyte solution. The photovoltaic effect is a phenomena in which a voltage or electrical current is generated in a material by being exposed to electromagnetic radiation. This is the basis of semiconductor photocatalysis and photoelectrochemistry.

Although the solar spectrum contains enough energy to conversion of radiant energy to electrical or chemical energy, this reaction does not occur spontaneously at significant rates, due to the low absorption coefficient in the UV-visible region of the electromagnetic spectrum. However, in theory, sunlight can be used to excite a semiconductor material, which in turn acts as a catalyst for conversion of radiant energy to electrical or chemical energy. In practice, the progress in the photoelectrochemical conversion of radiant energy to electrical or chemical energy technology is materials-limited. The most challenging key factors are the existence of a material with a band gap suitable for capturing as much energy as possible from incident light, its stability in a wide range of aqueous electrolytes and minimization of charge carrier recombination. Further, the material has to be in a plentiful supply and environmentally benign for scalable applications. To this end, metal oxide semiconductors appear to exhibit superior properties as photo-electrodes in comparison to other types of materials. Titania is one of the possible materials for the energy conversion because of its excellent photocatalytic activity [25].

2.3 Introduction of TiO₂

Recently, Owing to titanium dioxide (TiO₂) has relatively high photocatalytic activity, biological and chemical stability, low cost, non-toxic nature and long-term stability, it is one of the most widely semiconductors, many researchers have been studied it in many fields such as sensing devices, solar cell and waste water treatment.

2.3.1 Basic Properties

TiO₂ is a n-type semiconductor and has three common polymorphs: anatase (tetragonal) in low temperatures, rutile (tetragonal) and brookite (orthorhombic) in high temperatures. Moreover, anatase and rutile are most used in photocatalytic reaction, and anatase gives better reaction activity than rutile. It is conjectured that the Fermi level of anatase ($E_G = 3.2$ eV) is higher than rutile ($E_G = 3.0$ eV). Some basic properties of three crystal structures of TiO₂ are shown in Table 2.1 [35]

Table 2.1 Basic properties of three crystal structures of TiO₂ [35]

	Anatase	Rutile	Brookite
Crystalline	Tetragonal	Tetragonal	Orthorhombic
Specific Gravity (g/cm³)	3.9	4.2	4.13
Mohs Hardness	5.5-6.6	6.0-7.0	6.0-6.5
Dielectric	31	114	-
Index of Refraction	2.52	2.71	-
Energy Gap (eV)	3.2	3.0	3.2
Melting Point (°C)	Transform into rutile at 600 °C	1,858	1,770 (Transform into rutile in high temperature)

2.3.2 Morphology and Fabrication of Nano-Scale TiO₂

A variety of preparation routes have been used to fabricate nano-scaled TiO₂ of different geometric shapes and microstructures such as wires, dots, particulates and tubes. Among one-dimensional architectures, nanotube arrays have a higher surface area than nanowires and nanoparticles due to the additional surface area enclosed inside the hollow structure. Hence, many researchers have great interest in fabricating TiO₂ nanotubes. Moreover, TiO₂ nanotubes have been fabricated by electrochemical anodization [36], template method [37], and hydrothermal synthesis [38] as follows:

(1) Template Method

The preparation of nanotubes by template method is shown schematically in Figure 2.1. Anodic aluminum oxide (AAO) template has attracted much interest for the preparation of several nanosized materials [37]. The size of TiO_2 nanotubes can be controlled by applied templates. However, the template method is gradually superseded, because there are some difficulties, such as complex fabrication and post-removal, yet to overcome.

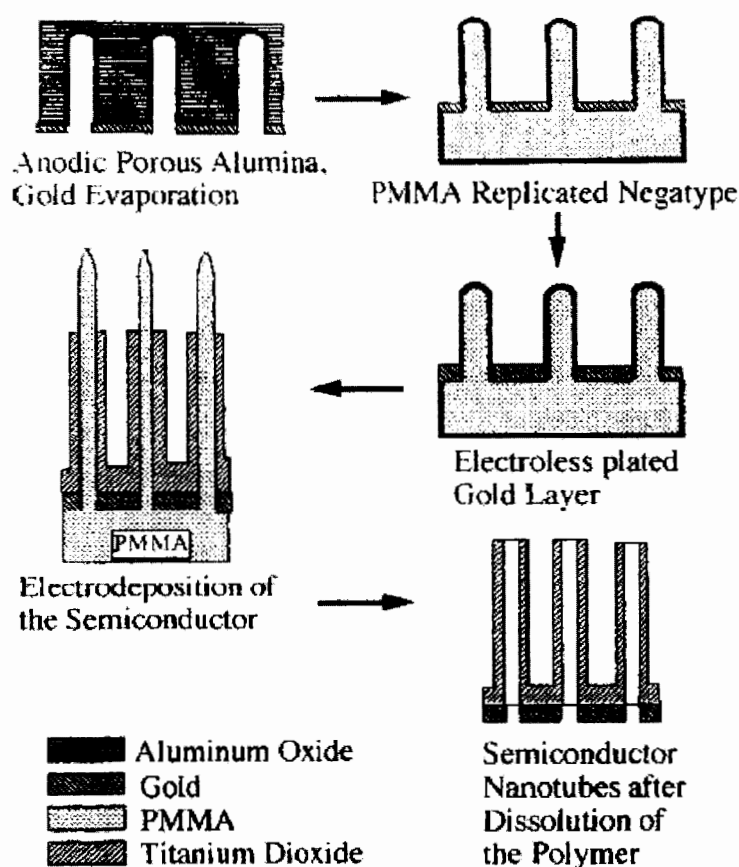


Figure 2.1 Preparation process of TiO_2 nanotube by template method [37]

(2) Hydrothermal Synthesis

After the innovative achievements from Kasuga et al. [38], the fabrication of TiO_2 nanotubes by hydrothermal synthesis has promoted vigorous research activities. TiO_2 nanotube can be synthesized from the TiO_2 particles in highly concentrated NaOH solutions. A schematic diagram for the formation of TiO_2 nanotubes by hydrothermal synthesis is shown in Figure 2.2. The key factors affecting

the fabrication of TiO₂ nanotube arrays by hydrothermal synthesis were temperature and duration of treatment, alkali solution, Ti precursors and acid washing [39]. The hydrothermal synthesis is suitable for large scale production of low dimensional, well separated and crystallized TiO₂ nanotubes.

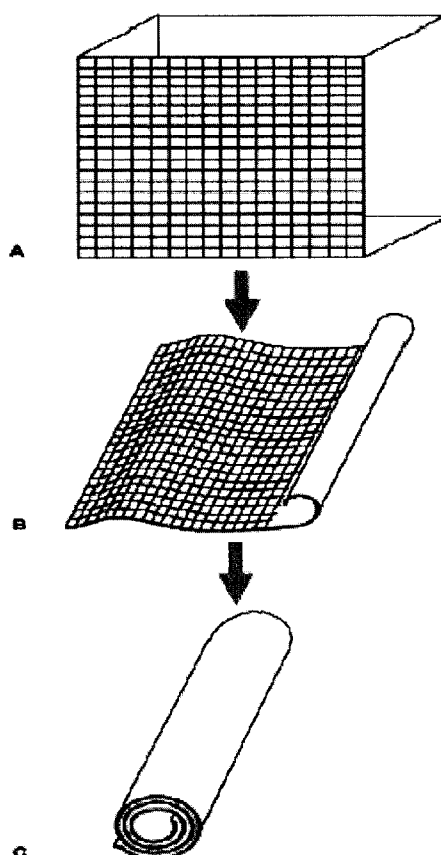


Figure 2.2 Schematic diagram for the formation of TiO₂ nanotubes by hydrothermal method [40]

(3) Electrochemical Anodization

TiO₂ nanotube arrays fabricated by anodic oxidation in electrolytes containing fluoride possess many excellent properties such as highly-ordered, uniform diameter and length, effective contact with Ti foil, high aspect ratio using anodic oxidation method. A schematic set-up for anodic oxidation is shown in Figure 2.3. TiO₂ nanotube arrays are tubular structure which can increase the light scattering. Moreover, it not only increases the light absorption, but also shows much higher

conversion efficiency than TiO_2 nanoparticle, owing to its high electron transporting characteristics. Therefore, TiO_2 nanotube arrays fabricated by anodic oxidation have been considered for extensive applications such as photocatalysts, dye-sensitized solar cells and gas sensors. There are several operational variables associated with the fabrication of TiO_2 nanotube arrays, such as anodization voltage, water content in electrolyte, anodization time, anodization temperature, fluorine ion concentration, pH value of electrolyte and annealing environment. In this studied, we will focus on electrochemical anodization.

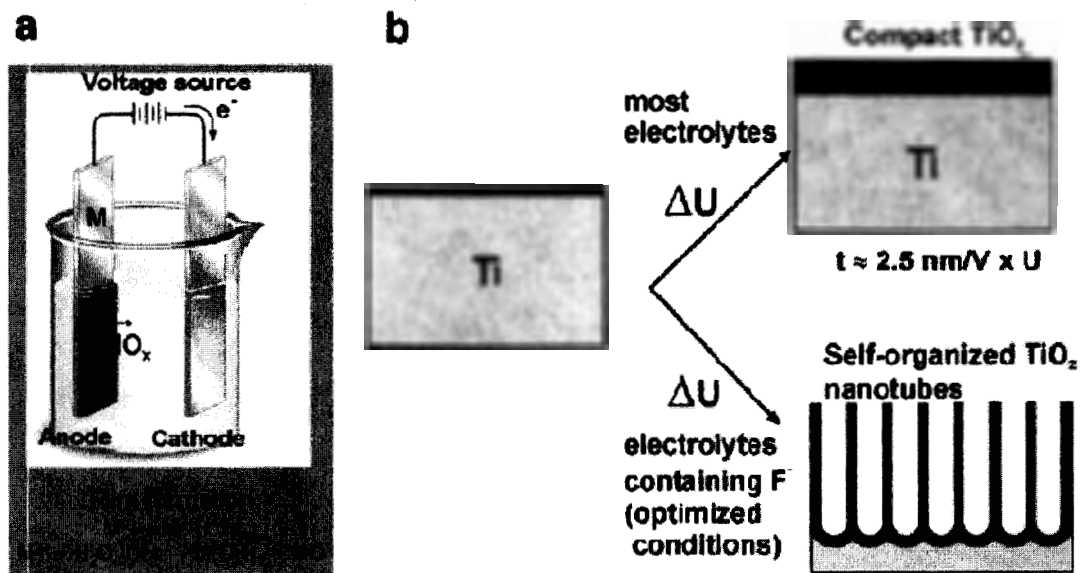


Figure 2.3 The schematic set-up for anodic oxidation method [36]

2.4 Nanostructures material

A nanostructure is a structure of intermediate size between microscopic and molecular structure. Nanoscience and technology are considered to be the materials with the dimensions ranging from several nanometers to several hundred nanometers. The main types of nanostructured materials based on the dimensions of their structural elements are zero-dimensional (0D), one-dimensional (1D), two-dimensional (2D) and three-dimensional (3D) nanomaterials, as illustrated in Figure 2.3. Zero-dimensional nanomaterials include nanocluster materials and nanodispersions, such as materials in which nanoparticles are isolated from each other. One-dimensional nanomaterials

are nanofibre or nanorod and nanotubular materials with fibre length from 100 nm to tens of microns. Two-dimensional nanomaterials are coating films with nanometer thickness. Structural elements in 0D, 1D and 2D nanomaterials can be distributed in a liquid or solid macroscopic matrix or be applied on a substrate. Three-dimensional nanomaterials include powders, fibrous, multilayer and polycrystalline materials in which the 0D, 1D and 2D structural elements are in close contact with each other and form interfaces. An important type of three-dimensional nanostructured materials is a compact or bulk polycrystal with nanosize grains, whose entire volume is filled with those nanograins, free surface of the grains is practically absent, and there are only grain interfaces. The formation of such interfaces and disappearance of the nanoparticle or nanograin surface is the fundamental difference between three-dimensional compact nanomaterials and nanocrystalline powders with various degrees of agglomeration that consist of particles of the same size as the compact nanostructured materials.

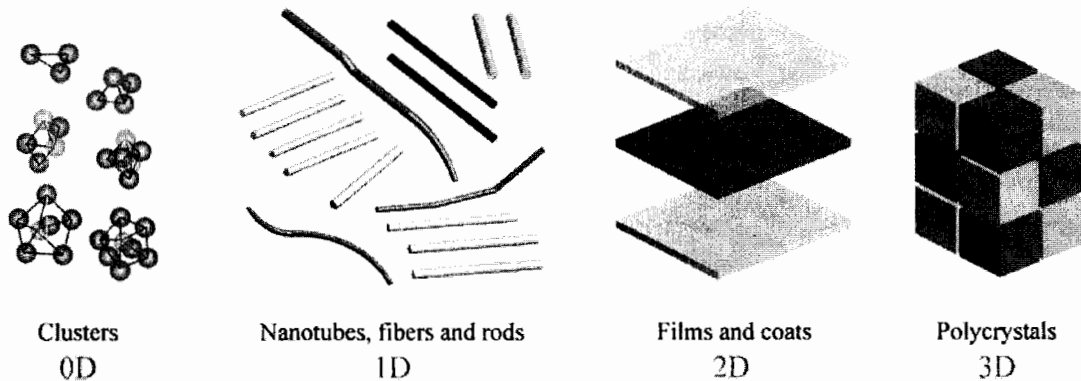


Figure 2.4 Types of nanocrystalline materials by size of their structural elements: **0D (zero-dimensional) clusters; 1D (one-dimensional) nanotubes, fibers and rods; 2D (two-dimensional) films and coats; 3D (three-dimensional) polycrystals.** [99]

One of the very basic results of the physics and chemistry of solids is the insight that most properties of solids depend on the microstructure, i.e. the chemical composition, the arrangement of the atomic structure and the size of a solid in one, two or three dimensions. In other words, if one changes one or several of these parameters, the properties of a solid vary. The most well-known example of the correlation between the atomic structure and the properties of a bulk material is probably the spectacular variation in the hardness of carbon when it transforms from diamond to graphite. Comparable variations have been noted if the atomic structure of a solid deviates far from equilibrium or if its size is reduced to a few interatomic spacing in one, two or three dimensions [26].

New and interesting physical and chemical properties emerge when the size of a material decreases down to the nanometer domain. Properties also vary as the shapes of the shrinking nanomaterials change, the surface area and number of bonds on the surface increases. In semiconductor materials within this size domain, the movement of electrons and holes is governed by the well-known quantum confinement effect, and the transport properties related to phonons and photons are largely affected by the size and geometry of the material. As a result, quantum confinement has an effect on the optical, electrical, and chemical functionalities. Quantum confinement effect in nanomaterials is a result of a dispersed distribution of allowable energy states. That is, as the size of the particle a decrease in dimension from bulk to nano-sized, the density of states (DOS) becomes discreet. A review article by Xiaobo Chen, and Samuel S. Mao [27] covers numerous synthesis methods to achieve nanosized titanium dioxide, while an extensive review by Ulrike Diebold [29] covers the bulk properties and surface science of titanium dioxide. Although there are several methods to synthetically obtain 1D titania nanostructures such as nanotubes, nanorods, generally three methods are hydrothermal synthesis, template directed growth using porous alumina, and electrochemical anodization. Out of these three methods, electrochemical anodization offers several advantages over the former two. For example, electrochemical synthesis is a scalable process, offers easier reagent handling, and demonstrates robust control on the nanoscale. In the former two synthesis methods, the final material is in powder form, which can limit its applications. Electrochemical synthesis methods have shown promise to synthesize a number of metal oxide

nanostructures, in particular electrochemical anodization of so-called valve metals and their alloys. Through the use of various processing techniques, a wide variety of nanostructures can be synthesized with high control. The synthesis of vertically orientated self-ordered metal oxide nanotube arrays on metal substrates, using electrochemical anodization technique, has been reviewed [34-36], as well as their application in solar energy conversion systems [37-39].

2.5 Mechanism of Titania Nanotube arrays formation by anodization method

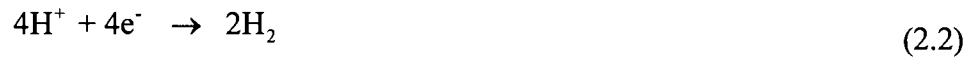
The key processes responsible for anodic formation of titania nanotube arrays are oxide growth at the metal surface due to interaction of the metal with O^{2-} or OH^- ions which decomposed from the bulk electrolyte and reacted with metal ion (Ti^{4+}) to form the initial oxide layer. Moreover, these anions will continuously react with Ti^{4+} ions by diffusing through the oxide layer and reaching the metal or oxide interface. On the other hand, Ti^{4+} ions will migrate to metal or oxide interface and further be progressed to oxide or electrolyte by applied electric field [45]. When increasing anodization time, oxide layer become more thickness by Ti^{4+} ions dissolve into the electrolyte and O^{2-} anions migrate to the metal or oxide interface. Moreover, electrochemical dissolution process will react at the same time and form small pits on the surface of oxide layer. Owing to pits causing relatively thinner barrier layer, at bottom, the electric field intensity across the bottom of pits was increased [42-44]. Continued the above reaction, the pits progressively deepen and widen to form the pores indicated that the deeper pores will cause uneven electronic charge distribution over oxide and the protruded metallic regions will form inter-pore voids by local electric field. Due to pore and voids form, they will compete for the available current and finally both voids and tubes grow in equilibrium [41].

The anodic growth of compact oxides on the surfaces of titanium sheets and the formation of nanotubes can be explained by following reactions:

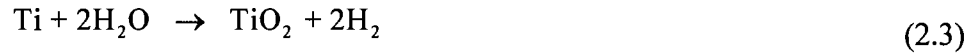
At the anode, there action takes place:



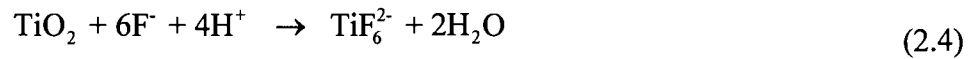
At the cathode, hydrogen evolution occurs:



The overall process of oxidation formation is given by:



Fluorine ions can attack the oxide and hydrated layer or the ions being mobile in the anodic layer under the applied electric field, react with Ti^{4+} as described by:



The formation of tubular structures is shown in Figure 2.5. The anodization onset a thin layer of oxide forms on the titanium surface Figure 2.5a. Small pits originate in this oxide layer due to the localized dissolution of the oxide Figure 2.5b making the barrier layer at the bottom of the pits relatively thin which, in turn, increases the electric field intensity across the remaining barrier layer resulting in further pore growth, Figure 2.5c. The pore entrance is not affected by electric field assisted dissolution and hence remains relatively narrow, while the electric field distribution in the curved bottom surface of the pore causes pore widening, as well as deepening of the pore. The result is a pore with a scallop shape [44-45]. The pits progressively deepen and widen to form the pores indicated that the deeper pores will cause uneven electronic charge distribution over oxide and the protruded metallic regions will form inter-pore voids by local electric field, Figure 2.5d. Due to pore and voids form, they will compete for the available current and finally both voids and tubes grow in equilibrium, Figure 2.5e. The nanotube length increases until the electrochemical etch rate equals the chemical dissolution rate of the nanotube top surface. After this point is

reached the nanotube length will be independent of the anodization duration, as determined for a given electrolyte concentration and anodization potential.

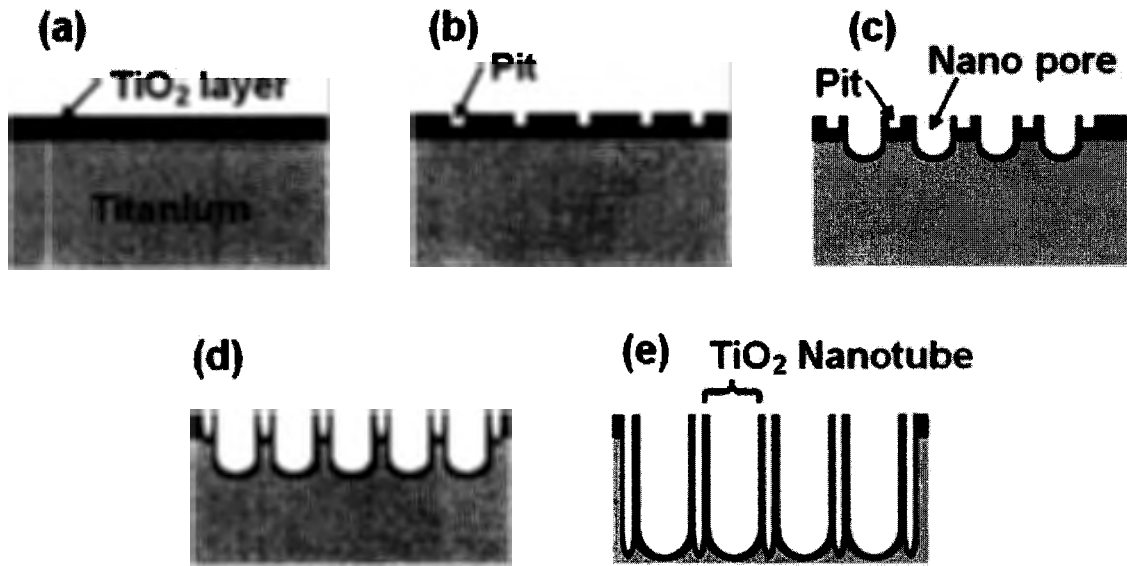


Figure 2.5 The formation of tubular structures [53].

2.6 Fabrication of TiO₂ Nanotube Arrays by Electrochemical Anodization

The effect of operational parameters on the morphology and dimension of nanotube arrays are discussed as follow.

2.6.1 Effect of Anodization Voltage

Anodizing voltage is one of the factors to affect electrochemical oxidation rate and electrochemical dissolution. The electrochemical oxidation rate increases with increasing anodizing voltage and affects the growth of TiO₂ nanotube arrays. Therefore, it is an important driving force to occur anodization process.

Albu et al. (2008) [46] prepared TiO₂ nanotube arrays with organic electrolyte containing ethylene glycol, HF and H₂O₂ at varied anodizing voltage of 120, 40 and 0 V. They found a very regular layer with thickness of about 10 mm forms that consists of aligned, individual TiO₂ nanotubes with diameters of 150 nm was formed with anodizing voltage of 120V. Moreover, if anodizing voltage is lowered to 40 V, and the growth of the nanotubes slows down, depending on the resulting conditions, may entirely stop.

Liu et al. (2008) [47] found that the anodizing voltage influences the nanotube formation process and morphology of the as-anodized samples greatly. At a lower voltage resulted a compact oxide layer, there are no exact tubular structure formed and the nanopores was highly disordered with average pore diameter smaller than 15 nm. On the contrary, at a higher voltage, nanotubular structures can be identified and small disordered, due to the insufficient growth of the oxide film, and the partial irregular nanotubes should be related to general chemical etching of the tubular walls. Moreover, the author said the nanotubular structure will be almost destroyed when the anodizing voltage was higher than 30 V.

Liu et al. (2009) [48] investigated the effect of the applied potential on the microstructure of the as-prepared nanotubes under ultrasonication condition, the anodizing voltage was applied from 5 V to 20 V with the electrolyte composition contained 0.5 wt% HF solution and anodization time (1800 s) constant. Furthermore, their studies found that anodization at 5 V for 1800 s only gives a thin layer of porous film rather than nanotube, but the voltage increased to 20 V, the anodization results nanotubes layer with diameter and length of about 65 and 280 nm, respectively. It is evidenced that both the diameter and length increased with an increment in applied potential.

2.6.2 Effect of Anodization Time

Anodizing time is affecting the length of TiO₂ nanotube arrays and playing an important role in anodization process. As shown in Figure 2.6, Albu et al. (2008) [46] investigated the current-time curve during anodiaztion process, in first stage a compact oxide layer forms and as time goes on the current drops exponentially with increasing layer thickness. At step II, a fine porous layer forms due to the layer is partially etched by fluoride ion migration and accompanying oxide dissolution and the current increases. In the third stage the reaction is stabilized, and regularly growing pores or tubes are formed. Therefore, anodization time plays an important role for growth of TiO₂ nanotube arrays and the length of TiO₂ nanotube arrays increases with the increasing anodization time.

Liu et al. (2009) [49] prepared TiO₂ nanotube arrays by anodization process under ultrasonic wave irradiation for different time intervals ranging from 10 s to 3600 s at 20V. When anodization time over 500 s, a tube-like surface morphology was

obtained and there are well-aligned nanotubes ~ 280 nm in length, ~ 65 nm in inner diameter and ~ 5 nm in wall-thickness after anodization time to 1800 s. Moreover, they found that with further anodization, there is almost no further change in the nanotubular structure when anodization process extended from 1800 s to 3600 s.

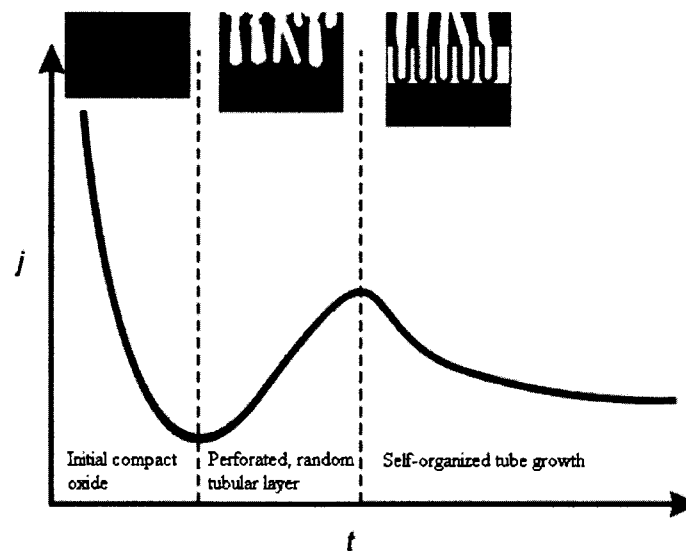


Figure 2.6 Typical current-time characteristics and corresponding growth stages during anodization process [46]

Yoriya et al. (2009) [50] investigated TiO₂ nanotube arrays by anodization process, the anodization electrolyte were diethylene glycol mixing with HF. They found at the first 20 h, TiO₂ nanotube arrays growth rate is +0.2 μm/h, and +0.4 μm/h is obtained from 20-40 h anodization duration, owing to the oxidation growth rate is faster than the oxide dissolution. On the contrary, when anodization time beyond 40 h, the oxide dissolution is faster than the oxidation growth rate and the tube length decreases with a negative growth rate of -0.1 μm/h.

Kuang et al. (2008) [51] studied highly ordered TiO₂ nanotube arrays with ethylene glycol electrolyte containing 0.25 wt% H₂O and 0.75 wt% NH₄F for different anodization time. The result revealed the average TNT lengths are 5-14 μm increasing with increasing anodization time from 2-2 h.

Hattori et al. (2011) [52] prepared TiO₂ nanotube arrays in glycerol electrolyte containing 0.5 wt% NH₄F for different anodization duration and annealed at 450 °C in air for 90 minutes. Anodization time at 1 hr and 10 hr, length of TiO₂ nanotube arrays from 150 nm increased to 1.5 μm, but dimension showed the same inner pore (~23 nm) and outer diameter (~36 nm). However, anodization time at 30 hr, dimension of TiO₂ nanotube arrays increased to 45 nm and 55 nm. When anodization time increasing up to 36 hr, TiO₂ nanotube arrays showing oblique geometry.

2.6.3 Effect of Water Content in Electrolyte

Owing to the anhydrous nature of the ethylene glycol, many researchers will add specific amounts of deionized water as an additional electrolyte component. Hence, the water content significantly affects the morphology of TiO₂ nanotube arrays and the influences of water content on growth of TiO₂ nanotube arrays are described as following:

Prakasam et al. (2007) [53] studied morphology of TiO₂ nanotube arrays with electrolyte containing different concentration of H₂O from 1 to 3 vol% for a 17 anodization at 60 V. They found at the 0.3 wt% NH₄F, the length of TiO₂ nanotube arrays reached maximum at the H₂O concentration of 2 vol%. Moreover, water is usually the source of oxygen in anodizing solutions. When more water is present, hydroxyl ions will injected into the body of the oxide layer and affect the structure sufficiently to inhibit ion transport through the barrier layer. On the contrary, when less

water is present, the rate of growth of the overall oxide film will be limited, owing to the difficulty in extracting oxygen and/or hydroxyl ions.

Alivov et al. (2009) [54] prepared TiO₂ nanotube arrays in glycerol electrolyte with NF₄F and H₂O at different anodization voltages (V_a) and electrolyte composition. They indicated addition of water to the electrolyte results in an increase in TNT growth rate and modification of TNT film morphology. The result revealed there was poor dependence of the diameter on the voltage at low H₂O concentration (< 5%); however there was a very well pronounced linear dependence of the diameter on the voltage at higher water concentration (≥5%). Owing to addition of water decreases the electrolyte viscosity, so this parameter seems to be crucial for NT diameter control.

2.6.4 Effect of Fluorine Ion Content in Electrolyte

Fluoride content is one of the important factors to affect anodization process, owing to the electrochemical dissolution was the fluoride ion reacting with titanium dioxide to form the [TiF₆]²⁻. Many researchers studied the relationship between electrochemical dissolution and the formation of TiO₂ nanotube arrays by different dosage of ammonium fluoride on anodization process.

Macák et al. (2005) [55] prepared TiO₂ nanotube arrays by 1M Na₂SO₄ solutions with the addition of different amounts of NaF (0.1-1 wt %) and they found that anodization in NaaSCU solution containing 0.1 and 0.3 wt% of NaF results in the etch reaction happened but etch is not uniform on the entire surface. Moreover, anodization process in Na₂SO₄ (1 M) solution containing NaF in the range of 0.5-1 wt % results in far more uniform porous structures. When the concentration of NaF is higher than 1 wt %, it will be not produced due to the limited solubility of NaF in aqueous solution of 1M Na₂SO₄. Furthermore, in their studied indicated that pore size is not significantly depending on the NaF concentration.

Prakasam et al. (2007) [53] studied morphology of TiO₂ nanotube arrays with electrolyte containing different concentration of NE₄F from 0.1-0.3 wt% and anodization for 17 h at 60 V. They found at the 2 vol% H₂O, the length of TiO₂ nanotube arrays increased at the concentration of NH₄F increasing up to 0.3 wt%. Furthermore, at concentration of ammonium fluoride lower than 0.3%, the reaction rate is low and the water absorbed from the ambient sufficient to meet the demand for

oxygen arising from the TiO₂ nanotube formation. NH₄F concentration greater than 0.3 wt % without water addition resulted in corrosion on the foil directly.

Wang et al. (2009) [56] studied the concentration of HF is too high, the oxide layer on the surface of TiO₂ nanotube arrays will be easily etched, leaving an over etching pores and excess HF may continuous etching the structure of TNTs, resulting in a large number of defects. Moreover, the concentration of HF is one of the factors affected the rate of chemical etching. Therefore, they increasing the concentration of HP up to 10 vol% confirmed that the length of TNTs further decreased due to the rapid etching of TNTs both in the vertical direction and in the lateral direction.

2.6.5 Effect of Temperature

The influence of temperature of electrolyte on the performance of growth TiO₂ nanotube arrays depends on electrochemical oxidizing rate and chemical dissolution rate. Especially, chemical dissolution rate is a temperature dependent process with etching rates typically being exponential functions of the temperature [57]. Hence, the morphology of TiO₂ nanotube arrays was affected by anodization temperature.

Mor et al. (2005) [57] investigated TiO₂ nanotube arrays which anodized at 10 V in electrolyte bath of four different temperatures: 5, 25, 35 and 50 °C. However, they found that the wall thickness increases with decreasing anodization temperature from 9 nm at 50 °C to 34 nm at 5 °C. Moreover, when decreases electrolyte bath temperatures the wall thickness increases and in the same diameter the wall thickness increases will cause tubes becoming more interconnected result in each nanotubes look like a nanoporous structure on the surface. On the other hand, the length of the nanotubes (corresponding to the thickness of the nanotube layer) increases with decreasing anodization bath temperature from 120 nm at 50 °C to 224 nm at 5 °C.

Wang et al. (2009) [56] prepared TiO₂ nanotube arrays in the 0.5 wt% NH₄F and 1 vol% HF ethylene glycol electrolyte solution anodized at 60 V for 1 h with various anodization temperatures from -5 to 60 °C. They found that the reaction temperature can affect the chemical etching and the electrochemical anodization, especially the chemical etching at the early stage and the electrochemical anodization

at the late stage. At the late stage, chemical etching also will affect by concentration of HF, because consumption of HF will make it slower. In brief, anodization temperatures can control nanoporous and nanotubes morphology, the pore size, the wall thickness, and the nanotubes length.

2.6.6 Effect of Electrolyte pH Value

It is well known that the growth of TiO₂ nanotube arrays from a competition between chemical dissolution and electrochemical oxidizing. The electrolyte pH value is one of the factors to affect chemical dissolution rate. Hence, in order to know the influence of pH value on the growth of TiO₂ nanotube array, many researchers studied the anodization under various pH values in electrolyte.

Macák et al. (2005) [55] studied the effect of pH value on the dissolution of TiO₂ etching experiments. In their studied found when pH of electrolyte solution is 2, there is highest dissolution rate observed and the rate approximately 38 nm/min. On the contrary, electrolyte solution at pH= 5 the dissolution rate is the lowest with a rate of less than 1.5 nm/min. Therefore, it is evident that in acidic electrolytes the rate of chemical etching is much higher than in alkalinity electrolytes.

Sreekantan et al. (2009) [58] investigated well-organized TiO₂ nanotubes by anodizing titanium foil in 1 M Na₂SO₄ containing 0.3 g of NH₄F. They found nanotube lengths ranging from ~0.7 to 2.5 μm could be formed by altering the electrolytes pH. Moreover, with increasing pH value the rate of formation decreasing obviously and the rate as follow: pH 3 at a rate of 23 nm mm⁻¹, 0.7 μm; pH 5 at a rate of 15 nm min⁻¹, 0.6 μm; pH 7 at a rate of 8 nm min⁻¹, 0.5 μm.

From previous literature revealed that the nanotube-array length was subsequently increased to about 7 μm by control of the anodization electrolyte pH (higher values while remaining acidic) which reduced the chemical dissolution of TiO₂ during anodization.

2.7 Factors Affecting Utilizing TiO₂ Nanotube Arrays

2.7.1 Annealing Condition of TiO₂ Nanotube Arrays

At first, owing to the prepared TiO₂ nanotube arrays is amorphous, we have to transform it into crystalline, in order to facilitate photocatalytic reaction. There are three common polymorphs in TiO₂ nanotube arrays: anatase in low temperature, rutile

and brookite in high temperature. In the past literatures, anatase and rutile are most used in photocatalytic reaction, and anatase gives better reaction activity than rutile. Moreover, the ratio between them is important to result photocatalytic efficiency. Therefore, photocatalytic efficiency will different from different annealing condition,

Allam et al. (2010) [59] fabricated TiO_2 nanotube arrays by anodization process with a formamide-based electrolyte containing 0.2 M NH_4F , 1 M H_3PO_4 , and 3 vol% H_2O at 20 V for 20 h. The as-anodized samples were crystallized by oxygen annealing at different temperatures with heating and cooling rates of 1 $^\circ\text{C}/\text{min}$. In their studied, the anatase-to-rutile phase transformation was found to start at 550 $^\circ\text{C}$ and annealed temperature up to 700 $^\circ\text{C}$ rutile still does not transformation completely. However, the anatase-to-rutile transformation starts near 430 $^\circ\text{C}$ for the 500 nm long nanotubes studied by Varghese and coworkers. Therefore, they indicated the nanotube length is a factor to effect phase transformation process.

Awitor et al. (2008) [60] prepared TiO_2 nanotube arrays by anodization with electrolyte containing 0.4 wt% HF at room temperature (20 $^\circ\text{C}$) and the voltage maintain at 20 V. The as-anodized sample annealed at different temperature 300 - 600 $^\circ\text{C}$ in increments 50 $^\circ\text{C}$ and oxygen for 1h. They found the morphology of TiO_2 nanotube arrays are not affected by increasing annealed temperature to 500 $^\circ\text{C}$. Moreover, annealed temperature up to 550 $^\circ\text{C}$ and 600 $^\circ\text{C}$, the anatase-to-rutile mass ratio decreased to 30:70 and 20:80, respectively.

Schulte et al. (2010) [61] prepared TiO_2 nanotube arrays in the 1 M H_2SO_4 and 0.8 M KF electrolyte solution with adjusted pH = 4.0 and anodized at 20 V for 2 h. The as-anodized samples were annealed in ambient air at different temperatures with heating rates of 1 $^\circ\text{C}/\text{min}$. They found the barrier oxide layer below the nanotubes is beginning to convert to rutile at 480 $^\circ\text{C}$ and fully converted to rutile at 620 $^\circ\text{C}$. When annealed temperature is up to 680 $^\circ\text{C}$, the nanotube structures are collapse. Moreover, in CO_2 reduction reaction the sample annealed at 680 $^\circ\text{C}$ has the best photocatalytic activity, due to the collapsed nanotube will created new active site. However, the oxidation reaction resulted that anatase is more usefully oxidant compared with rutile and the sample annealed at 550 $^\circ\text{C}$ has the best photocatalytic activity, due to anatase/rutile has the best ratio.

2.7.2 Dimension of TiO₂ Nanotube Arrays

In previous studies indicated that dimension of TiO₂ nanotube arrays can be controlled by different anodization processes, such as various anodization time or different anodization potential. Recently, many researchers studied photocatalytic efficiency with TiO₂ nanotube arrays prepared by different anodization processes as follow:

Smith et al. (2009) [62] prepared TiO₂ nanotube arrays by anodization process in ethylene glycol containing 0.5 wt% NH₄F and 10 wt% H₂O with various anodization potential from 20 - 60 V. They indicated the diameter of TiO₂ nanotube arrays can be easily changed by varying the applied potential during the anodization process and an average tube diameter are 50 to 120 nm. The results revealed the increase in diameter improves the conversion. However, increasing the diameter from 75 to 120 nm does not proportionally improve the dye conversion.

Liu et al. (2009) [49] prepared different dimension of TiO₂ nanotube arrays by anodization process with changed anodization potential and anodization time. The result in a nanotube arrays approximately 19.4 μm in length, referred as long tube. As a comparison, the short TiO₂ nanotube arrays, about 500 nm in length. In photocatalytic reaction, removal efficiency of methylic orange (MO) reaches 63.1% for long nanotube electrode after 3 h reaction, which is much higher than 46.9% for short nanotube electrode. It is possible that long nanotube possess larger specific surface area than short nanotube. In photoelectrocatalytic reaction, removal efficiency of MO for long nanotube electrode is also better than short nanotube electrode. Owing to long nanotube electrode has a large effective surface area in close proximity with the electrolyte solution, thus the photo-generated electrons can transfer more effectively to the counter electrode via the external circuit. Therefore, the long nanotube electrode can be improved due to the effective separation of electron-hole pairs on the surface of electrode.

Lai et al. (2006) [63] investigated TiO₂ nanotube arrays by electrochemical anodization in 0.5 wt% HF with various potential at 10-20 V for 20 minutes. It can be observed that lengths and inner diameters of TiO₂ nanotube arrays are 215-400 nm and 38-78 nm, respectively. They indicated that with increasing dimension of TiO₂ nanotube arrays, the rate of methylene blue removal was increased. Moreover, the

results revealed increased anodization there are higher active anatase phase ratio, light absorption ability, and greater UV response arrangement. Moreover, the increasing amounts of TiO₂ participating to generate more photoelectrons and holes in heterogeneous photocatalysis.

2.7.3 Applied Bias Potential

The bias potential is shown an important factor influencing the photoelectrocatalytic reactions. Owing to the structure of TiO₂ nanotube arrays is vertical tube and connect compactly with Ti substrate, it can provide a unidirectional electric channel. Therefore, many researchers are interesting in photoelectrocatalytic reaction by utilizing TiO₂ nanotube arrays.

Quan et al, (2007) [64] investigated photoelectrocatalytic degradation of pentachlorophenol by utilizing TiO₂ nanotube film electrode with various bias potential. They applied four levels of bias potential, 0.0, 0.2, 0.4 and 0.6 V, respectively. In photoelectrocatalytic reaction, bias potential supply draws the photoinduced electrons to the counter electrode. Therefore, bias potential is a key factor that affects PEC efficiency. Moreover, when the bias potential applied from 0.0 to 0.6 V, pentachlorophenol removal w|§ increased and from previous literature indicated electrochemical degradation and water splitting requiring a potential greater than 0.6 V. Hence, the enhancement of PCP photodegradation was not due to direct electrochemical degradation or secondary reactions caused by active oxidizing free radicals such as free hydroxyl radicals produced by electrochemical water splitting, but was mainly due to charge separation.

Brugnera et al. (2010) [65] studied effect of bias potential on the BPA degradation kinetics and choosing the best condition. Bias potential varied from -0.6 to +1.5 V and the result revealed the initial degradation rates increased with the applied potential and maximum degradation rate was obtained at E = +1.5 V. Moreover, applied bias potential supplied an electric field, which keeps photogenerated charges apart. These results also suggest that adsorption of the BPA is enhanced and/or the generation and separation of electron-hole pairs is accelerated under the field gradient, which promotes faster BPA decomposition.

Wu et al. (2009) [66] investigated enhancing photoelectrocatalytic degradation of methylene blue by applied different bias potential: 0.0, 0.2, 0.4 and 0.6 V, respectively. In direct electrocatalytic oxidation with potential at 0.8 V found that no noticeable degradation of MB was detected in the presence of NaCl but without illumination. However, in the case of photoelectrocatalytic reaction, with a relatively low applied potential of +0.6 V, almost completed degradation (about 97.57%) was observed at 60 minutes. Because applied bias potential generates a bending of the conduction band, it causes a more effective charge separation to increase the photocurrent, and likely promotes a better oxidative degradation process.

2.7.4 Modification of TiO₂ Nanotube Arrays

Owing to the relatively large band gap of TiO₂ limits the efficiency of photocatalytic reaction, the photogenerated electron and hole will recombination easily. Currently, many researchers paid their attention on highly ordered TiO₂ nanotube arrays loaded with noble or transition metals because TiO₂ nanotube arrays has extensively applications such as gas sensor, dye-sensitized solar cell and photocatalyst. Moreover, TiO₂ nanotube arrays loaded with metal can increase photocatalytic efficiency and expand absorption in visible light region.

Sun et al. (2009) [67] introduced Fe³⁺ dopant into the highly ordered TiO₂ nanotube array film during ananodization process. They indicated that enhanced of photocatalytic activity attributes to the effective separation of photogenerated electron-hole upon the introduction of appropriate Fe³⁺ amount into the anatase TiO₂ structure.

Lai et al. (2010) [68] fabricated Nitrogen-doped TiO₂ nanotube arrays by a wet immersion and annealing post-treatment. They found the annealing temperature and the light source used for the degradation experiment strongly effect the photocatalytic activity of N-doped TiO₂ nanotube arrays. Moreover, The N-doped TiO₂ nanotube array films annealed at 450 °C have the highest photocatalytic activity to degrade MO pollutant under visible (0.027 min⁻¹) or UV light (0.169 min⁻¹) sources.

Liu et al. [69] investigated short nanotube electrode doped CdS by sonoelectrochemical deposition method to improves the combination between CdS and TiO₂ nanotubes, as well as the dispersion of CdS nanoparticles. The result revealed the presence of CdS nanoparticles significantly extends the response of TiO₂

nanotubes in the visible region. Moreover, CdS can facilitate the separation and transfer of photogenerated electron/hole pairs. Photocurrent of CdS/TiO₂ electrode enhanced to ~7 fold in comparison with the pure TiO₂ nanotube electrode.

Xie et al. (2010) [70] prepared Ag nanoparticles loaded TiO₂ nanotube arrays by pulse current deposition. They found the maximum incident photon to charge carrier efficiency value of Ag/TiO₂ nanotube arrays was 51 %, much higher than pure TiO₂ nanotube arrays. Moreover, Ag/TiO₂ nanotube arrays exhibited higher photocatalytic activities than the pure TiO₂ nanotube arrays under both UV and visible light irradiation. The photoelectrocatalytic activity of Ag/TiO₂ nanotube arrays was increasing 1.6 times in comparison with the pure TiO₂ nanotube electrode.

Zhang et al. (2011) [71] studied photocurrent density and the photocatalytic degradation efficiency of Ag loaded N-doped TiO₂ nanotube arrays. They revealed the average photocurrent density and the photocatalytic degradation efficiency of the Ag/N-TNTs obtained for the degradation of Acid Orange II are 6 times and 6.8 times higher than those of annealed TiO₂ nanotube arrays.

2.8 Doping Titania Nanotube arrays

One of the major challenges for scientific communities includes the proper application of titania nanotube arrays under visible light. Visible light composes the largest part of solar radiation. Anatase TiO₂, which is the most photoactive phase of TiO₂ only absorbs ultraviolet light with wavelengths shorter than 380 nm which occupies only about 5% of solar energy [72].

The solar radiation in space is relatively independent of the position. The terrestrial sunlight radiation intensity, however, depends on the zenith angle. The solar radiation that reaches the Earth's surface without being absorbed or scattered is called direct radiation. The sunlight that is scattered in the atmosphere is termed diffuse radiation. A measure of attenuation of sunlight in the atmosphere is air mass (AM) and this is related to the optical path length through the atmosphere determined by the zenith angle. The solar energy spectrum, determined for the common case of an air mass (AM) of 1.5. The solar energy spectrum, in terms of the number of photons as a function of photon energy, is shown in Figure 2.7.

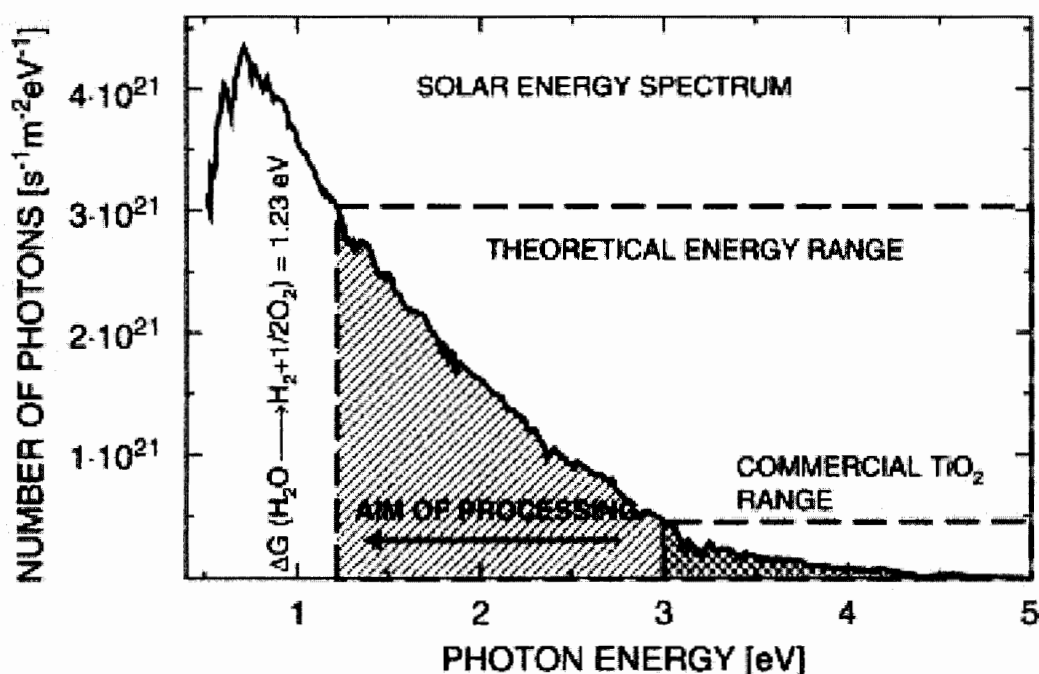


Figure 2.7 Solar energy spectrum for an air mass (AM) of 1.5 in terms of the number of photons as a function of photon energy, showing different photon flux regimes available for the conversion of solar energy (area under curve); band gap of commonly available TiO₂ and effect of band gap reduction through appropriate processing are also shown [73-74].

TiO₂ which is treated promising has been an attraction in the photocatalytic degradation of environmental pollutants and photoelectronchemical conversion of solar energy. TiO₂ is proved to be the most suitable photocatalysts for its non-toxicity, physical and chemical stability, and convenience for use. While the band gap of titania is about 3.0 eV for rutile phase and about 3.2 eV for anatase phase [75]. It can just be activated under ultraviolet (UV) irradiation, which the photon flux available for conversion is very small, which explains why the energy conversion efficiency (ECE) of these materials are low. So, there have been efforts to develop photocatalysts which need less energetic but more sufficiently visible light through band engineering of doping [73]. However, it has been shown that doping procedures used to reduce the E_g of TiO₂ do not lead necessarily to an increase in the ECE. As discussed, this failure is a result of increased energy losses associated with the fact that the ECE is determined

by several variables that must be modified simultaneously. This is why a research approach is essential. It also has been shown that most of these variables, such as electronic structure, charge transport kinetics and surface properties, are defect dependent. Therefore, defect disorder is emerging as the most suitable framework for the optimization of the performance of photoelectrodes based on metal oxides, including TiO_2 and its solid solutions [76]. Consequently, the subsequent papers in the present series concentrate on the defect chemistry of TiO_2 and those aspects of the defect chemistry that are associated with the photoelectrochemical properties of TiO_2 .

Over the past 10–15 years, considerable effort has gone into doping or band gap engineering of TiO_2 by introducing a secondary electronically active species into the lattice. The main thrust comes from photocatalytic or photovoltaic applications to exploit the solar spectrum much better and the onset energy for light absorption needs to be decreased [77]. The most typical methods to prepare doped TiO_2 nanostructures are retreating the final or growing TiO_2 nanomaterials in a solution or melt of the doping species, thermal treatments or synthesis in gas atmospheres of the doping species, production of the nanomaterials by co sputtering or sputtering in an atmosphere of doping species, high-energy ion implantation, and the use of a substrate of a suitable alloy or the incorporation of active electrolyte species for TiO_2 structures that grow from the metals by electrochemical oxidation.

In the band structure of TiO_2 made up of O 2p orbitals contribute to the filled valence band (VB), while Ti 3d, 4s, 4p orbitals contribute the unoccupied conduction band (CB). The lower position of CB is dominated by Ti 3d orbital. Upon doping with other cations in replacement of Ti, an impurity level could be introduced in the forbidden band. This intermediate energy level can act as either an electron acceptor or a donor, which allows TiO_2 to absorb visible light [78]. In silicon solar cells, doping is a frequently used method to improve conductivity. Here the effect can mainly be ascribed to the increase in free charges and thus conductivity, by the donation of electrons for dopants with a valency higher than that of the native material (n-type doping), or holes for dopants with a lower valency (p-type doping). In the case of TiO_2 the mechanism is much more complicated due to the defect ridden nature of TiO_2 and doping mainly affects the trap states and electronic structure of TiO_2 , which is illustrated by the improvements that are made by doping with elements of equal

valency as the host TiO_2 ions. Doping can be achieved by either replacing the Ti^{4+} cation or the O^{2-} anion. Cationic dopants are typically metals, whereas anionic dopants are non-metals. Since the lower edge of the CB is made up of $\text{Ti}^{4+}3d$ bands, replacing Ti^{4+} by a different cation is thus expected to heavily affect the CB structure. The upper edge of the VB consists of $\text{O}^{2-}2p$ bands and replacing O^{2-} by a different anion affects the VB energy [79].

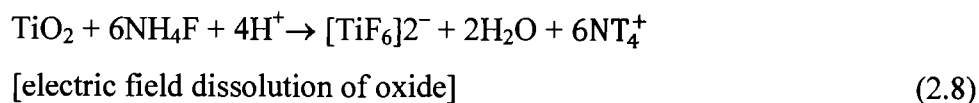
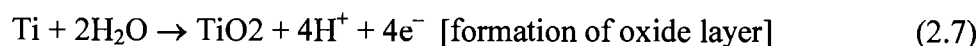
Dopants modify the electronic structure of nano- TiO_2 to broaden its effective range of light sensitivity for photocatalysis from the ultra-violet (UV) region to the visible light region [80]. Doping techniques have been shown to be effective and efficient despite their being susceptible to thermal instability and their requirement for expensive ion implantation facilities [81]. Dopants are valued for their ability to confer excellent physicochemical properties such as high crystallinity, high specific surface area, and small crystallite size [82-83]. There are three types of crystalline phases of nano- TiO_2 , namely, the rutile, anatase, and brookite phases. The anatase and rutile phases are the common crystallographic phases found in the formation of nano- TiO_2 , with the former particularly favored for its high photocatalytic activity [84] and exceptional thermodynamic stability in nanoscale dimensions [85]. The crystalline structure of nano- TiO_2 is represented as a TiO_6 octahedral. The formation of the anatase and rutile phases or phase transformation from anatase to rutile is strongly dependent on the thermal dehydration process during which time; Ti–O–Ti bonds are formed by the interaction between –OH groups and the protonated surfaces.

Specific surface area of TiO_2 is one of the factors that determine the morphology of TiO_2 in photocatalysis. A large specific surface area of TiO_2 enhances the photocatalytic degradation rate of organic pollutants as availability of active sites in TiO_2 is increased [86-88]. Crystallite size is another important characteristic that determines the quality of TiO_2 . The performance of nano- TiO_2 can be enhanced in the photocatalysis by producing nano-doped TiO_2 with high crystallite size up to a certain limit [88]. Then, the photocatalytic performance of nano-doped TiO_2 decreases when the crystallite size falls beyond this limit because of the trapping of charge carriers during the diffusion process. With the presence of dopants in the formation of nano-doped TiO_2 , the phase transformation from anatase to rutile inhibits when the thermal energy is low enough to overcome the nucleation barrier during the thermal

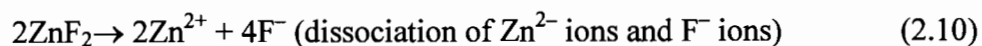
dehydration process, and this occurs more readily with the smaller crystallite size of nano-doped TiO₂ [88]. In short, dopants suppress the crystallite size of nano TiO₂ by inserting itself into the lattice structure of the nano-doped TiO₂ octahedral to modify its physicochemical properties. In general, a smaller crystallite size of nano-doped TiO₂ is favored compared to larger crystallite size of nano-doped TiO₂ since the smaller size reduces the recombination of the photogenerated charge carriers [80]. Some researchers reported that smaller crystallite size of nano-doped TiO₂ induced a larger band gap due to the increased redox ability [82]. The resultant photocatalytic activity benefits from the quantum size effect of nano-doped TiO₂ that enhances its photocatalytic activity [87].

2.9 Zinc incorporation of Titania Nanostructures

The formation of anodized NTs can be explained in terms of a competition between the oxidation of Ti into TiO₂ and field assisted dissolution of TiO₂ by F⁻ ions. The mechanism behind the formation of NT structures can be summarized in three initial processes described as (1) the formation of oxide (passivation layer) over the anode, (2) the electric field dissolution of oxide layer, which forms pits on the anode surface, and (3) the attack of F⁻ ion on these pits to form porous or tubular structure. It is also observed that not all but only selective pores transform into self-organized nanotubular structure [33]. These mechanisms can be defined by the following equations



To obtain Zn doped TiO₂-NTs, a freshly prepared solution of ZnF₂ with EG was used as an electrolyte. Here, ZnF₂ precursor forms negatively charged [ZnF₄]²⁻ complex, which under the influence of electric field drives to anode (Ti), where TiO₂-NTs have been formed. The formation of negative complex of ZnF₂ can be described as follows:



To investigate the effect of Zn doping on the formation of TiO₂-NTs and how the doping affects the other properties, two different concentrations of ZnF₂ were used while keeping the EG amount constant.

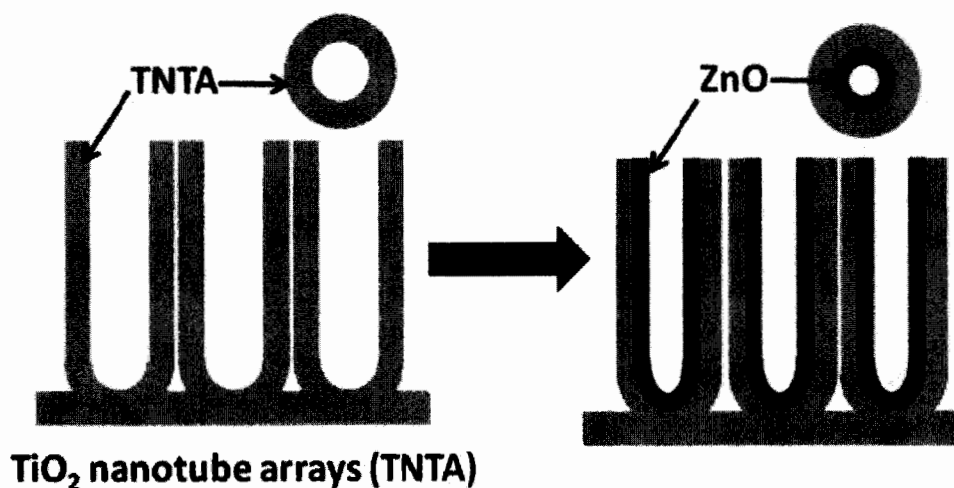


Figure 2.8A schematic of the preparation process for Zn doped TNTA.

A typical DSSC cell consists of two FTO, with a nanoporous TiO₂ layer covered with dye solution in the middle of the cell. Below it are the liquid electrolyte and the counter electrode that is usually fabricated with Pt. The mechanics of DSSC is quite different to the conventional silicon solar cell. The idea was initially inspired from the photosynthesis of the leaves. TiO₂, especially its anatase phase, has attracted much attention for its potential application in degradation of various environmental pollutants, both gaseous and liquid however; its short comings include a large band gap (~3.2eV) which causes most of the solar spectrum unutilized [89-91]. To extend the optical absorption of TiO₂ to the visible region, various dopants have been added to the oxide to improve its solar efficiency [92-93].

In this work we describe first the preparation of ZnO doped TiO₂ nanostructure, followed by the process of dye extraction from various parts of morphology and elementary composition of pure TiO₂, modified TiO₂ nanoparticles and by using XRD, SEM, and XPS analyses. Finally overall conversion efficiency for dye sensitized solar cells (DSSCs).

2.10 Dye sensitized solar cells (DSSCs)

Solar cells are photovoltaic devices that convert sunlight directly into electricity. The first generation solar cells, bulk-type c-Si based solar cells, suffer from complicated manufacture and high cost. The second generation solar cells that employ thin film technology can bring down the manufacture cost significantly, because of the extremely clean conditions required to process crystalline silicon. But their efficiency needs to be enhanced in order to make them practically viable. To reduce the manufacturing cost and increase the efficiency, a third generation solar cells that employ nanotechnology, such as dye-sensitized solar cells and organic solar cells have emerged [106-107]. Among the third generation solar cells, DSSCs attract great attention due to their higher solar cell efficiency.

A dye-sensitized solar cell (DSSCs) is a photochemical device that offers the potential of large-scale manufacturability at a competitive cost. A typical cell uses a liquid electrolyte or other ion-conducting phase as the charge-transport medium.

The actual dye-sensitized solar cell contains broadly five components are a mechanical support coated with Transparent Conductive Oxides, the semiconductor film, usually TiO₂, a sensitizer adsorbed onto the surface of the semiconductor, an electrolyte containing a redox mediator, and a counter electrode capable of regenerating the redox mediator like platine [94]. A schematic representation of the dye-sensitized solar cell is shown in Figure 2.9.

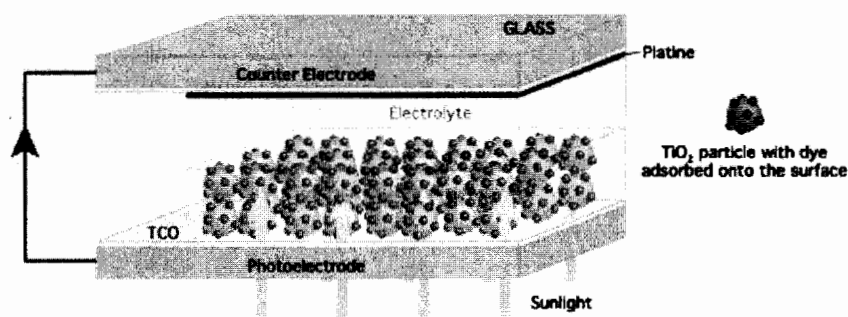


Figure 2.9 Schematic representation of the dye-sensitized solar cell [94].

The operating principle of DSSCs is comprised of a mesoporous oxide layer of anatase TiO_2 , the surface of which is sensitized with a monolayer of, typically, a ruthenium complex dye, for example, N719, N3, Black dye, anchored to the TiO_2 surface by a carboxylated bipyridyl ligand. The visible light absorption of these types of complexes is based on a metal-to-lig and charge transfer. The carboxylate groups are directly coordinated to the surface titanium ions producing intimate electronic contact between the sensitizer and the semiconductor. Photo-excited dye molecules inject electrons into the TiO_2 conduction band, and redox species such as the iodide/triiodide (I^-/I_3^-) couple in the electrolyte reduce the oxidized dye molecules back to their original state. Dye regeneration by the iodide happens through the thiocyanate group and, thereby, intercepts the recapture of the conduction band electron by the oxidized dye. In turn, the iodide is regenerated by the reduction of triiodide at the counter electrode, with the circuit completed via electron migration through the external load [96].

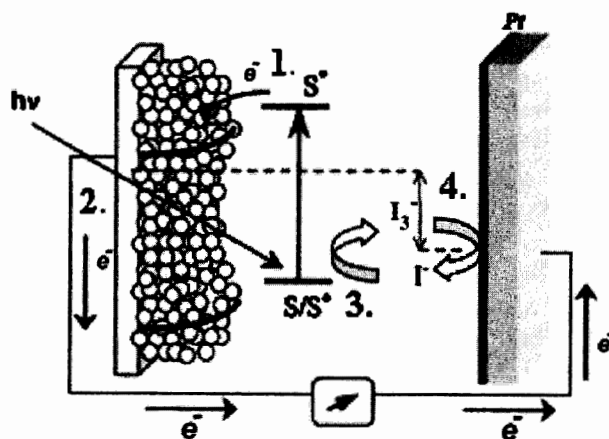


Figure 2.10 Operation principles and energy levels of nanocrystalline DSSCs [97].

The operational principle of DSSCs is illustrated in Figure 2.10. The system consists of the following [108]:

(1) Upon light absorption, the dye (S) is promoted into an electronically excited state (S^*) from where it injects, an electron into the conduction band of a large band gap semiconductor film (TiO_2), onto which it is adsorbed.

(2) The electrons are transported through the TiO_2 film by diffusion before reaching the anode of the cell.

(3) The positive charges resulting from the injection process are transferred into the liquid electrolyte by reaction of the dye cation (S^+) with the reduced species of a redox couple in the electrolyte solution. This leads to the generation of the charge neutral state of the sensitizer.

(4) The most typical redox couple is I^-/I_3^- . After ionic diffusion, the carrier of the positive charge (I_3^-) reaches the cathode, where it releases its charge thus being reduced back to I^- . When exposed to sunlight, the dye sensitizer gets excited from which an electron is injected into the conduction band of the mesoporous oxide film. These generated electrons diffuse to the anode and are utilized at the external load before being collected by the electrolyte at cathode surface to complete the cycle.

In order to enhance electrical conductivity and light transmittance, conducting glass is used as the substrate. There are mainly two types of conducting glass: indium-doped tin oxide (ITO) and fluorine-doped tin oxide (FTO). The standard to select a proper type is sometimes ambiguous because of the variety of cell configurations and materials. The semiconductor electrode is usually a layer of nanocrystalline titanium dioxide (TiO_2), a thin film deposited on the conducting glass film with the thickness 5–30 nm, which plays an important role in both the exciton dissociation and the electron transfer process. The porosity and morphology of the TiO_2 layer are dominant factors that determine the amount of dye molecules absorbed on its surface which can provide an enormous area of reaction sites for the monolayer dye molecules to harvest incident light. A large number of artificial dye molecules have been synthesized since the first introduction of dye-sensitized solar cells and some of them have already been successfully commercialized such as N3, N719 and Z907. Desirable dye molecules have to meet certain criteria, such as match with the solar spectrum, long-term operational stability, and firm graft on the semiconductor surface.

In addition, their redox potential should be high enough to facilitate the regeneration reaction with a redox mediator. As such, iodide and triiodide (I/I_3^-) redox couple is most commonly used in the liquid electrolyte, while other solid-state and quasi-solid electrolytes like organic hole-transport material and polymer gel are also applicable. Platinum is generally used as the cathode to catalyze the reduction of the oxidized charge mediator [98].

The overall performance of the above described solar cell can be evaluated in terms of cell efficiency (η) and fill factor (FF) expressed as

$$FF = \frac{V_{\max} J_{\max}}{V_{oc} J_{sc}} \quad (2.12)$$

$$\eta = \frac{V_{oc} J_{sc} FF}{P_{in}} \times 100\% \quad (2.13)$$

where J_{sc} is the short-circuit current density (mA/cm^2), V_{oc} is the open-circuit voltage (V), and P_{in} the incident light power (W). J_{\max} and V_{\max} correspond to current and voltage values, respectively, where the maximum power output is given in the J–V curve.

CHAPTER 3

EXPERIMENTAL PROCEDURES

In this chapter, I will describe the fabrication and characterization of ZnF_2 -doped titanium dioxide nanotubes (TiO_2 nanotubes) using anodization method for energy conversion. TiO_2 nanotubes will be studied characterization techniques used SEM, XRD, XPS, and testing of each sample's performance in a dye - sensitized solar cells (DSSC). The experimental procedure is summarized in Figure 3.1.

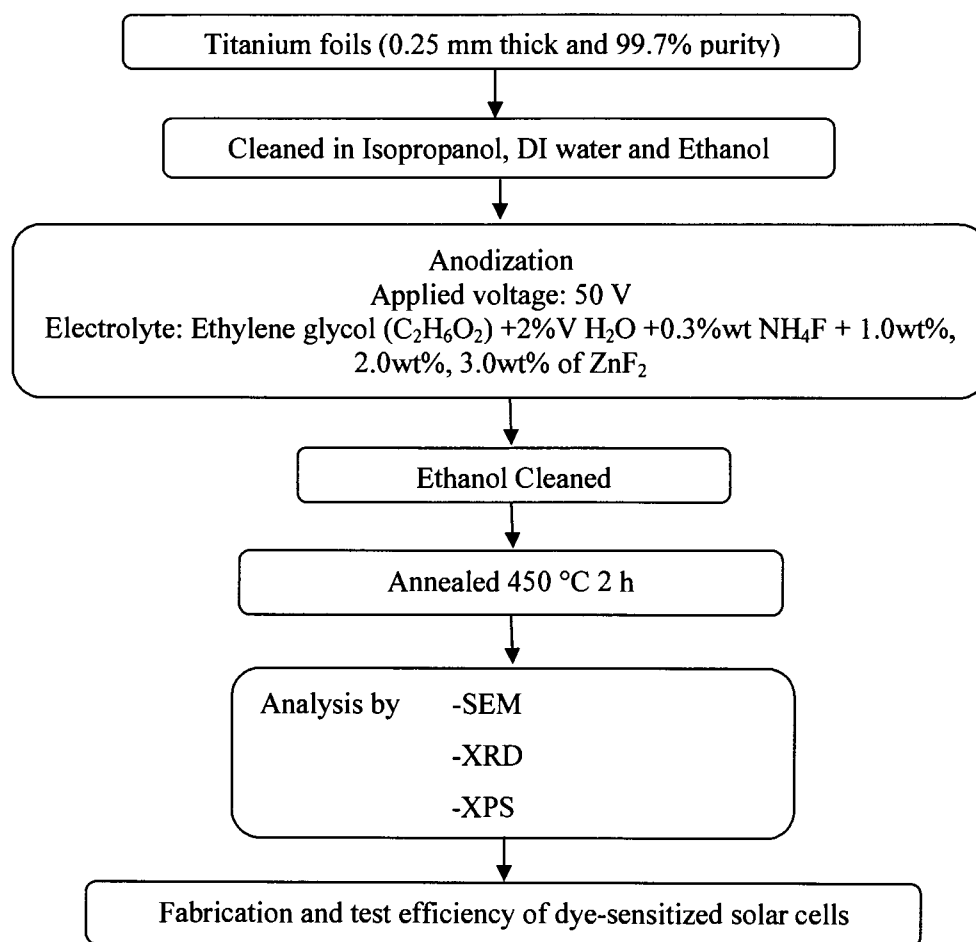


Figure 3.1 Flowchart of preparation of ZnF_2 doped TiO_2 nanotubes by anodization method for dye sensitized solar cells.

3.1 Materials and nanotubes preparation

The materials which were used in the experiments consist of Titanium (Ti) foil (0.25 mm thickness, 99.7% purity and Sigma Aldrich), ethylene glycol (EG), ammonium fluoride (0.3 wt % NH_4F), deionized water (2 Vol % H_2O) and Zinc Fluoride (ZnF_2). To clean the samples for growing ZnF_2 doped TiO_2 nanotubes, first, Ti foils were used as the substrates. Next, Ti foils were cut in circular shape with diameter of 2 cm to be served as substrates. The Ti substrates were degreased ultrasonically in the solution containing isopropanol, deionized water and ethanol with duration each 10 min respectively. Finally, the samples were dried in air and used immediately in the O-ring set in the electrolyte and electrodes container. The setup is then connected with a homemade power supply for anodization. Before the anodization, Ti substrates were mounted in a home-made housing. Only one face of the substrates was in contact with the electrolyte and was anodized. The system consisted of a two-electrode configuration with a piece of highly pure platinum counter electrode. The anode electrode was placed at the Ti foils. For, the cathode electrode is a platinum counter electrode by anidization in electrolyte.

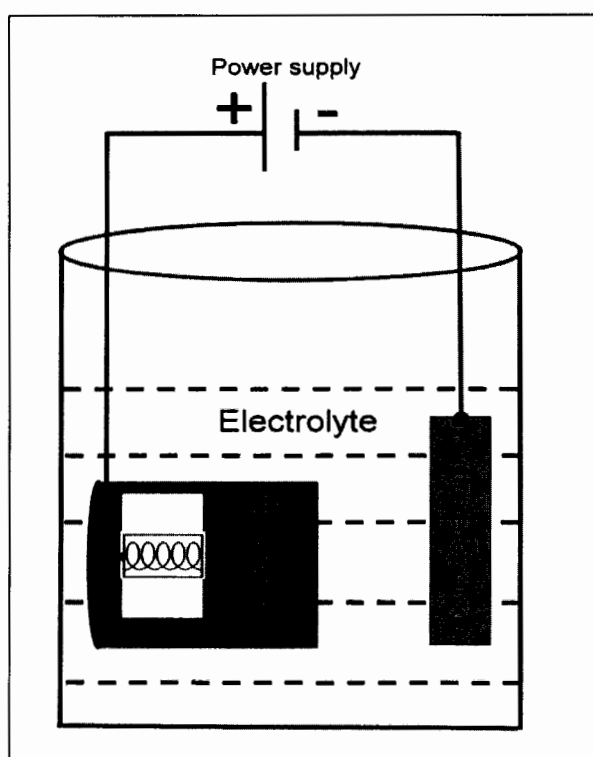


Figure 3.2 DC Anodization apparatus

3.2 Preparation of ZnF₂ doped TiO₂ nanotubes

In this research the TiO₂ nanotubes were prepared by DC anodization at room temperature on titanium sheet of thickness 0.25 mm, of diameter 2 cm and 99.7 % purity, purchased from Sigma Aldrich. Before anodization, the sheet was first polished and ultrasonicated for 10 minutes in isopropanol, de-ionized water and ethanol. The electrolyte solution which consist of ethylene glycol (EG), ammonium fluoride (0.3 % wt NH₄F) and deionized water (2 % vol DI H₂O), and doped 1.0 wt%, 2.0 wt% and 3.0 wt% of ZnF₂ was stirred magnetically for 2 hours and kept for 24 hours prior to anodization. The Ti sheet is mounted to serve as the anode in the electrolyte, while the cathode or counter electrode is made of platinum. A constant 50 V DC voltage is applied during anodization and each sample is anodized for 1 hours. This set up allows only one face of Ti foil contact with the electrolyte. And then, Ti foils were washed with ethanol and ultrasonicated to remove occluded ions from the surface of the TiO₂ nanotubes. The samples were annealed at 450 °C for 2 h. To investigate the surface morphology and nanostructure of ZnF₂ doped TiO₂ nanotubes all samples studied by SEM, XRD and XPS. The anodization set up is shown in Figure 3.3.

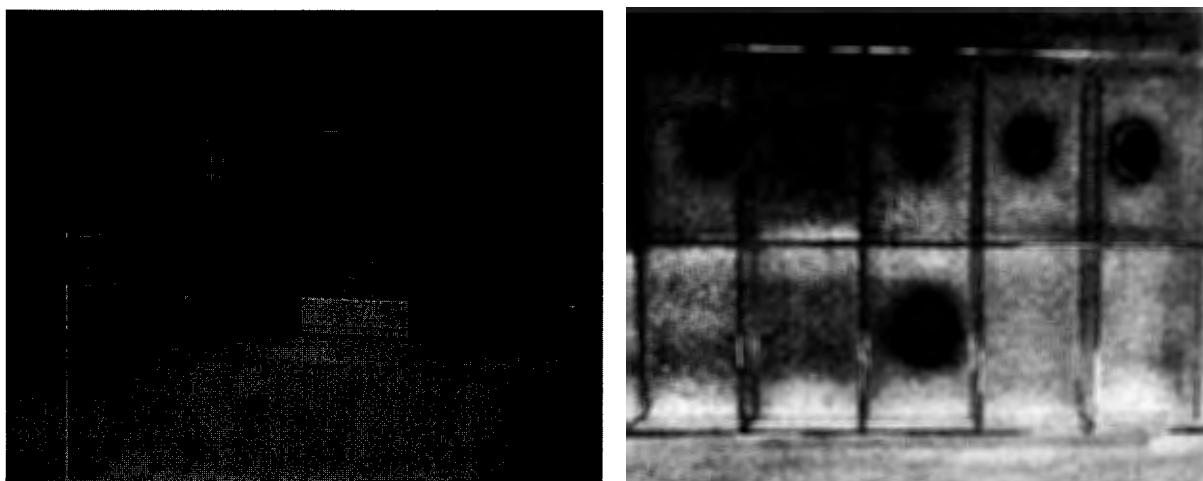


Figure 3.3 DC Anodization method and samples

3.3 Characterization Techniques of ZnF₂ doped TiO₂ nanotubes

The prepared samples were characterized using several techniques - Scanning Electron Microscopy (SEM), X-ray Diffraction (XRD), and X-ray Photoelectron Spectroscopy (XPS), and testing of each sample's performance in a dye - sensitized solar cell (DSSC).

3.3.1 Scanning Electron Microscopy (SEM)

The surface morphology of the samples was characterized using a JEOL JSM-6010 LV Scanning Electron Microscopy (shown in Figure 3.4) operating at an acceleration voltage of 20 kV.

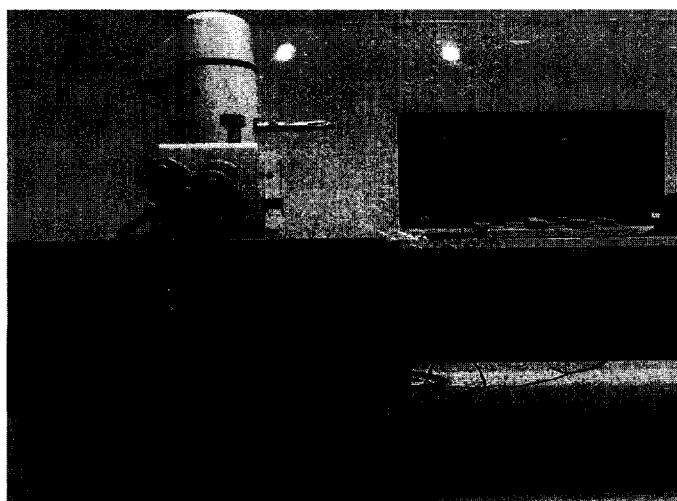


Figure 3.4 AJEOL JSM-6010LV Scanning Electron Microscopy

3.3.2 X-ray Diffraction (XRD)

The XRD was performed to determine the crystal phase and crystallite size of the samples using a Philips X'Pert-MDP X-ray diffractometer (shown in Figure 3.5) with Cu - K_α radiation ($\lambda = 1.5418 \text{ \AA}$) with Ni filter. The operational mode was 40 kV, 35 mA, with spectral scanning in the 2θ range from (20° - 80°) at a rate of 0.02° per second. Figure 3.5 shows a schematic diagram of how the X-ray Diffractometer operates.

Information about the crystal size D can be obtained from the XRD peaks. Given the X-ray wavelength (λ), the Bragg angle for the most prominent diffraction peak (θ), measurement of the full width half maximum (β), the crystallite size can be calculated using the Scherrer equation [37, 38]: Crystallite Size D

$$D = \frac{k\lambda}{\beta \cos\theta} \quad (3.1)$$

Usually, $k = 0.9$, and is called the shape factor or Scherrer constant.

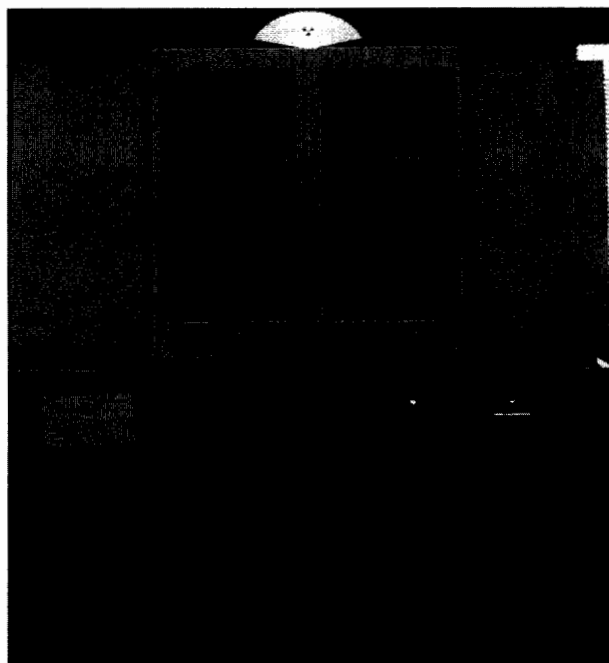


Figure 3.5 Philips X'Pert-MDP X-ray diffractometer

Lattice Parameter a

The diffraction of the incident waves through the crystal planes is illustrated in Figure 3.6. The distance d between crystal planes is given by Bragg's law [37, 38].

$$n\lambda = 2d \sin\theta \quad (3.2)$$

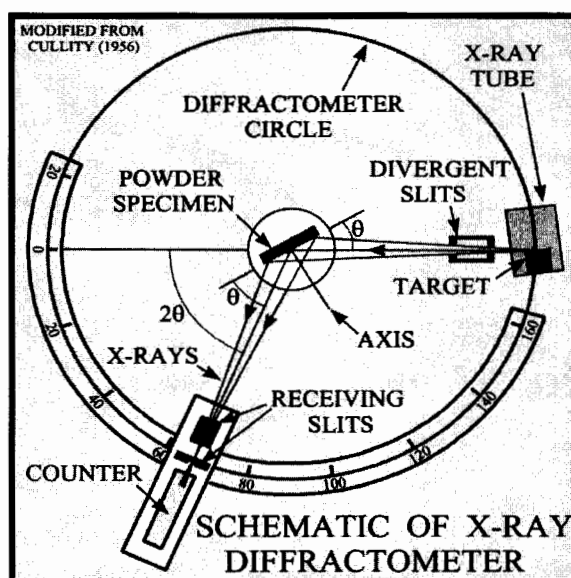


Figure 3.6 Schematic diagram of X-ray Diffractometer

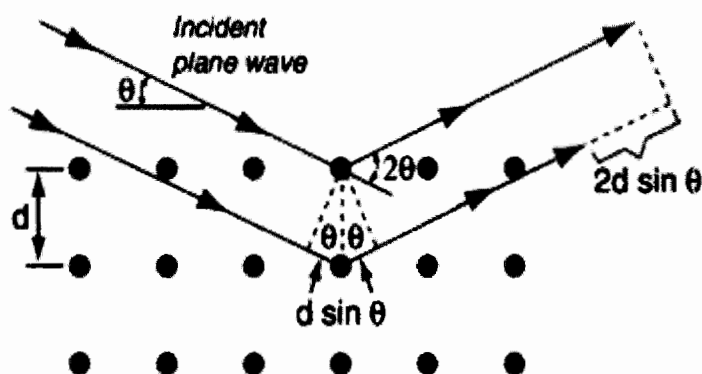


Figure 3.7 Bragg's law and diffraction through crystal planes

For cubic phases, each lattice parameter (a , b , c) can be determine using the Miller indices (hkl) of each reflection and the equation that follows [46]

$$a_o = d_{hkl} \sqrt{h^2 + k^2 + l^2} \quad (3.3)$$

Substituting Bragg's law gives

$$\sin^2 \theta = \frac{\lambda^2}{4a^2} (h^2 + k^2 + l^2) \quad (3.4)$$

The corresponding equation for a tetragonal crystal with axes a and c is given by

$$\sin^2\theta = \frac{\lambda^2}{4} \left(\frac{h^2+k^2}{a^2} + \frac{l^2}{c^2} \right) \quad (3.5)$$

The distance between crystal planes for a tetragonal crystal is given by

$$d_{hkl} = \frac{a}{\sqrt{h^2+k^2+(a^2/c^2)l^2}} \quad (3.6)$$

3.3.3 X-ray Photoelectron Spectroscopy (XPS)

XPS was used to determine the binding energy and elemental constituents present in the samples. Figure 3.8 shows the Thermo Al K- Alpha XPS machine (from South Korea) used for this research. XPS works on the photoelectric effect phenomenon. Low- energy X-rays are used to eject electrons from atoms. The binding energy E_B can be determined for an incident photon of frequency f , and ejected electron of energy E_e , using the following equation [3.8]:

$$E_B = hf - E_e \quad (3.7)$$

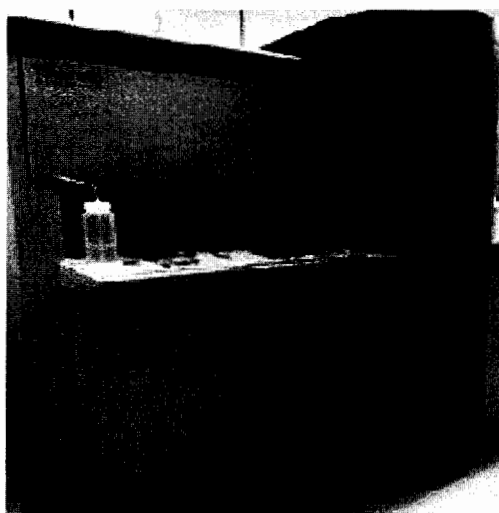


Figure 3.8 Thermo Al K- Alpha XPS machine (South Korea)

3.4 Fabrication and testing of a DSSCs

Titania nanotube films were immersed in 0.3 mM solution of N-719 dye in ethanol for 24 h to absorb the dye adequately. (The N719 dye 8.9 mg was dissolved in ethanol 25 ml). Afterwards, the dye sensitized TiO₂ films were rinsed with ethanol and dried in air.

A transparent conducting oxide glass (TCO) is used as counter electrode. After, TCO glass was cleaned with alcohol solution in an ultrasonic bath for 10 min and rinsed with DI water. A platinum catalyst was deposited on the TCO glass by coating with drop of platinum solution (H₂PtCl₆). The TCO glasses were heated for 30 min at 80 °C. And then, the TiO₂ nanotubes photoelectrode and Pt counter electrode were assembled into a sandwich. An electrolyte (KI/Iodine electrolyte) was injected into the cell. An electrolyte was prepared as following 0.6 M potassium iodide (KI) and 0.05 M iodine (I₂) were mixed with solvent of ethylene carbonate (EC) and propylene carbonate (PC) (6:4 v/v) under stirring to form a homogeneous liquid electrolyte solution.

After, the light was illuminated from the counter electrode. The cells have active areas of 0.25 cm². The current-voltage characteristic curves were measured with Electrometer Keithley2400 source meter. The Xenon arc lamp was used as an irradiation source and the intensity of the incident light was 100mW/cm². Measuring device of J-V curves for dye-sensitized solar cells is shown in Figure 3.9.

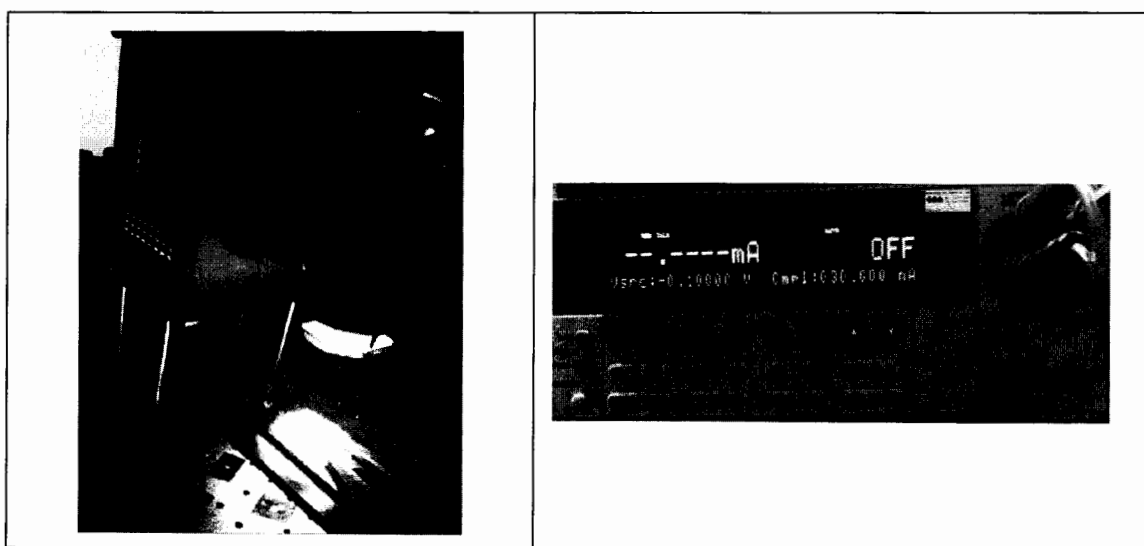


Figure 3.9 Shows measurement device of J-V curves for DSSCs.

The solar cells power conversion efficiency (η) is the parameter associated with the photovoltaic performance of the solar cell and defined as the ratio of the maximum power, (P_{\max}) to the incident light power, (P_{in}). The solar cell power conversion efficiency is defined as

$$\eta = \frac{P_{\max}}{P_{in}} = \frac{V_{oc} J_{sc} FF}{P_{in}} \times 100\% \quad (3.8)$$

where FF is the fill factor defined as

$$FF = \frac{P_{\max}}{V_{oc} J_{sc}} = \frac{V_{\max} J_{\max}}{V_{oc} J_{sc}} \quad (3.9)$$

where J_{sc} is the short-circuit current density (mA/cm^2), V_{oc} is the open-circuit voltage (V), and P_{in} the incident light power (W). J_{\max} and V_{\max} correspond to current and voltage values, respectively, where the maximum power output is given in the J–V curve.

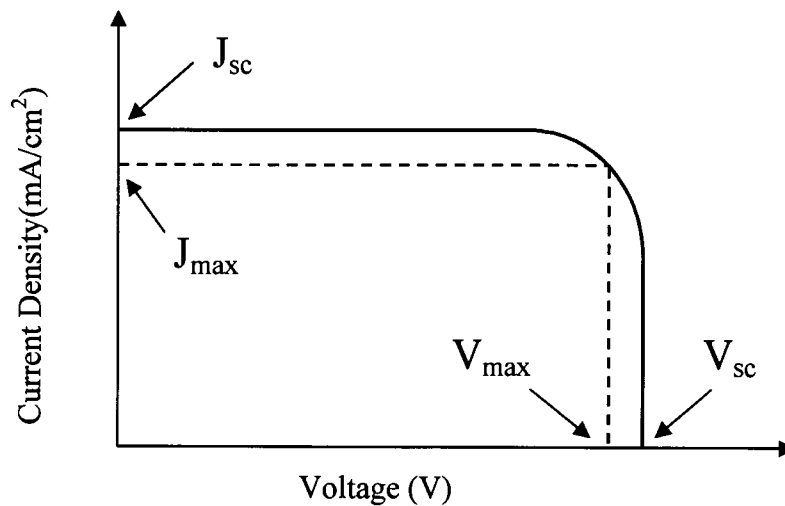


Figure 3.10 J-V curves for dye-sensitized solar cells.

CHAPTER 4

RESULTS AND DISCUSSION

In this chapter, I would like to present the experimental results of both undoped and ZnF₂ - doped TiO₂ nanotubes. The samples were analyzed by SEM, XRD, XPS, and tested in dye-sensitized solar cells (DSSCs).

4.1 Preparation and modification of Titania Nanotube arrays by anodization method

As anodized, the samples appear dark as shown in Figure 4.1.

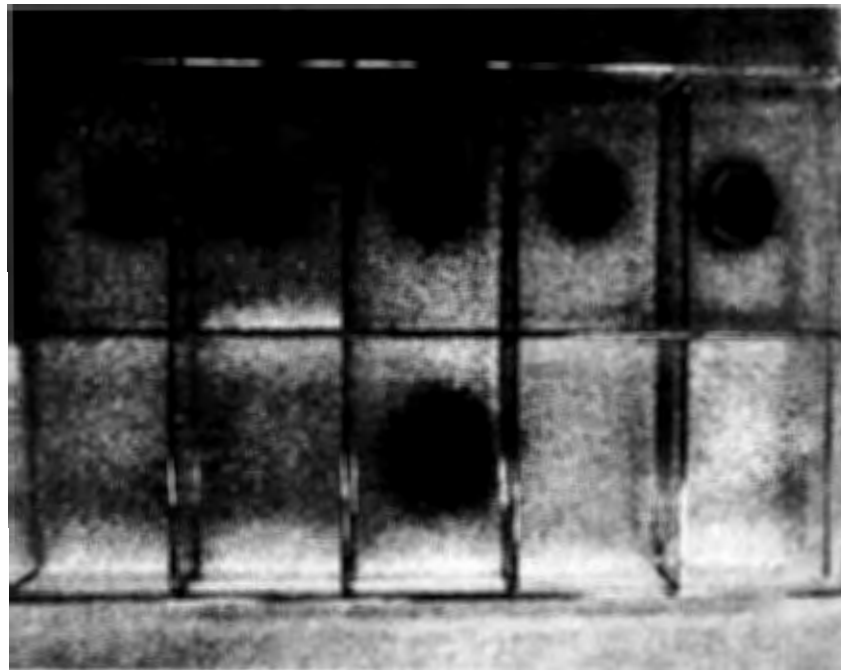
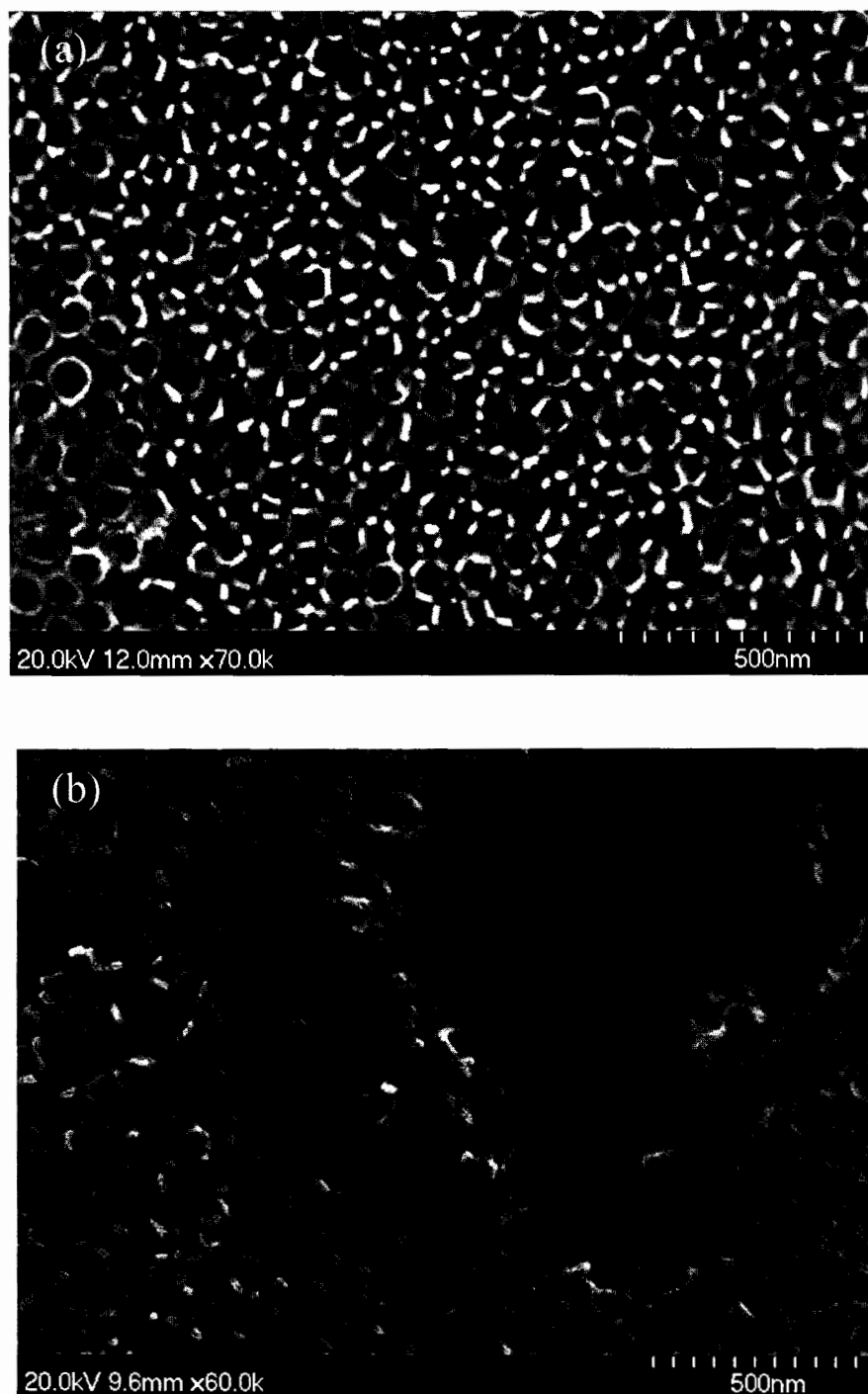


Figure 4.1 The Ti sheets were cut in circular shape with diameter of 1.4 cm.

4.2 Characterization of TiO₂ Nanotubes

4.2.1 SEM analysis



**Figure 4.2 SEM images of TiO₂ nanotube arrays with different doped ZnF₂:
Undoped (b) Doped 1.0 wt% of ZnF₂ (c) Doped 2.0 wt% of ZnF₂ and
(d) Doped 3.0 wt% of ZnF₂**

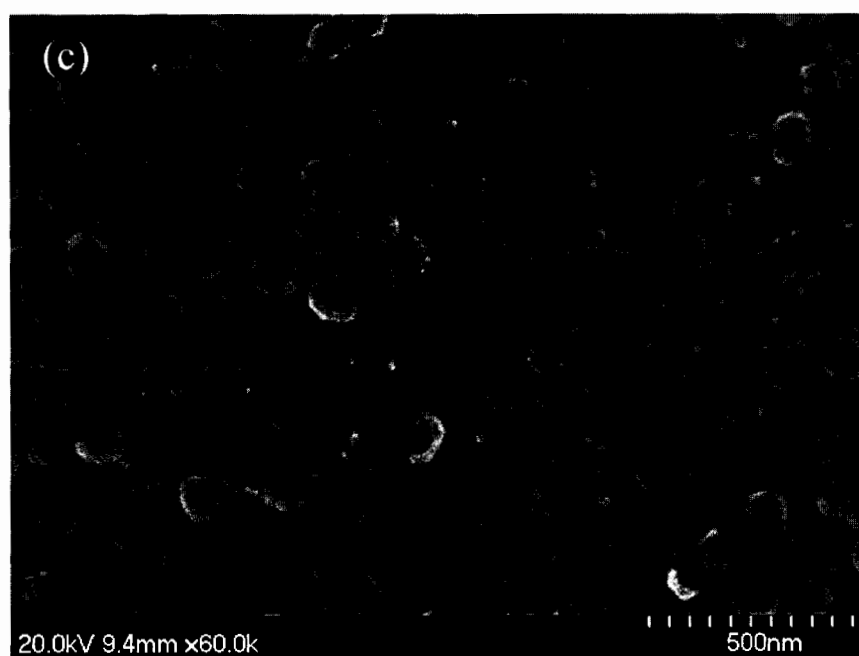


**Figure 4.2 SEM images of TiO₂ nanotube arrays with different doped ZnF₂:
Undoped (b) Doped 1.0 wt% of ZnF₂ (c) Doped 2.0 wt% of ZnF₂ and
(d) Doped 3.0 wt% of ZnF₂ (continued)**

The SEM images of TNTs doped with different concentrations of ZnF_2 are shown in Figure 4.1. The nanotubes are well-arrayed with an average diameter of about 66 nm, wall of about 15 nm, and approximately 1.47 μm in length.

The morphology of the pure and ZnF_2 doped TiO_2 nanotubes were studied by using SEM analysis and micrographs are shown in Figure 4.1 (a)-(d). It shows the synthesized TiO_2 nanotubes have average diameter of about 66 nm, wall of about 15 nm, and approximately 1.4740 μm in length. It shows the size of sample A (1.0 wt%), B (2.0 wt%), and C (3.0 wt%) synthesized nanotubes are increased compared to pure TiO_2 . It is clear that the prepared sample A, B, and C have tube shape and uniform size, good nanotube array all sample.

4.3 XRD Analysis

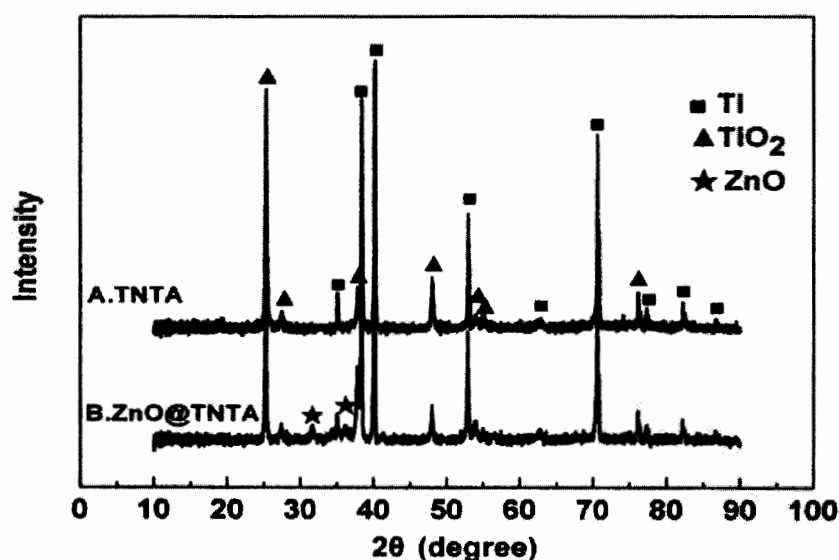


Figure 4.3 XRD patterns of TiO_2 nanotube arrays with ZnF_2 .

The structure of the ZnF_2 doped TiO_2 nanotubes was measured using XRD, as shown in Figure 4.3. The peaks of Zn, Ti and O are clearly identified, gives the XRD patterns of the TiO_2 nanotubes (TNTA: spectrum A) and ZnF_2 doped TiO_2 nanotubes (spectrum B). In spectrum A, the diffraction peaks are ascribed to TiO_2 and titanium substrate. Compared with spectrum A, new diffraction peaks at 31.6° and 36.1° emerge in the XRD pattern of ZnF_2 doped TiO_2 nanotubes (spectrum B), which

correspond to (100) and (101) plane of ZnO. In addition, the peaks of TiO₂ become weaker after the deposition of ZnO. The emergence of ZnO peaks and the weakening of TiO₂ peaks evidently confirm the successful growth of ZnF₂ doped TiO₂ nanotubes. The phase of TiO₂ nanotubes is anatase.

4.4 XPS patterns

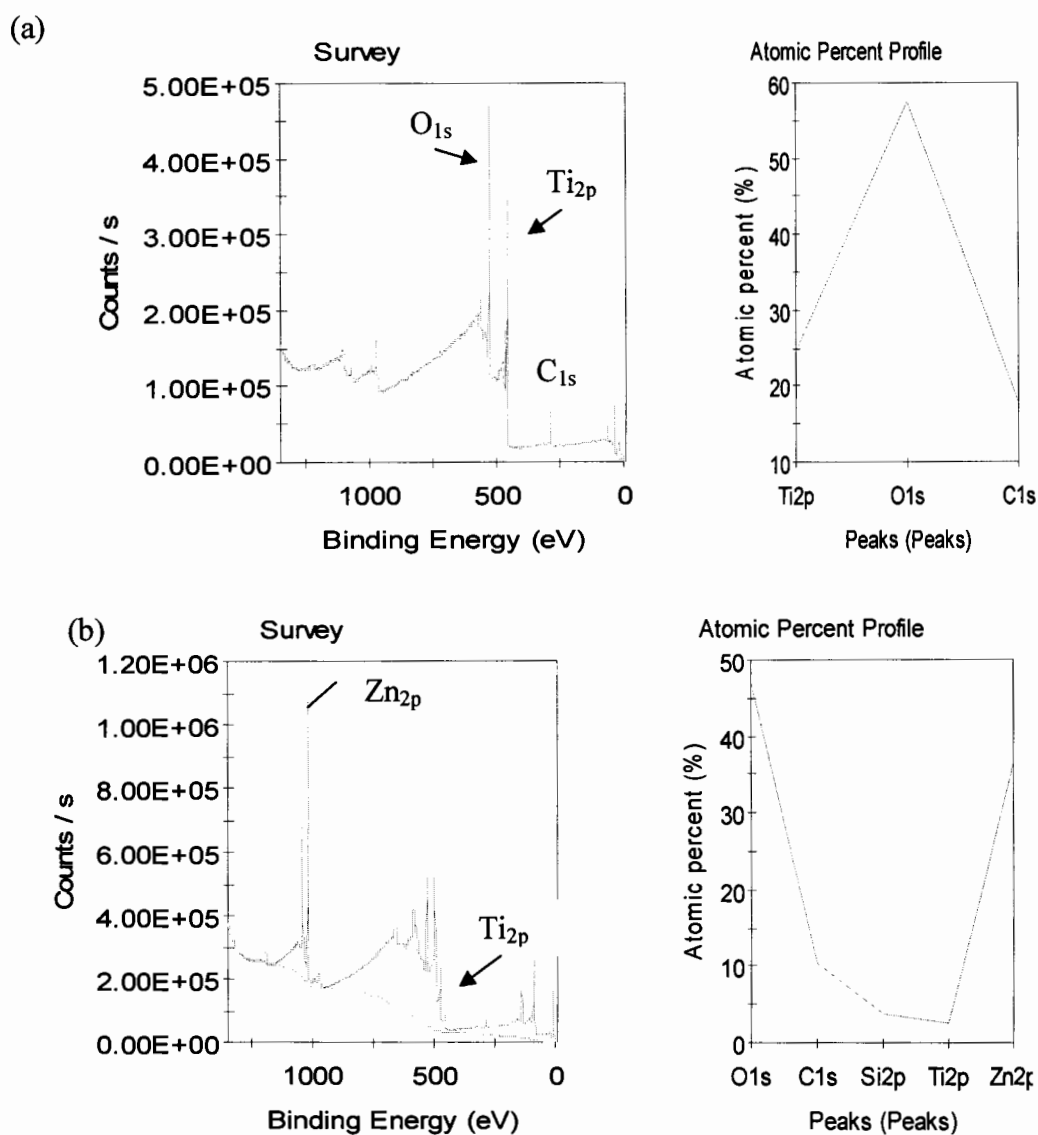


Figure 4.4 XPS spectra of ZnF₂ doped TiO₂ nanotubes with different doped ZnF₂: (a) Undoped (b) Doped 1.0 wt%, of ZnF₂ (c) Doped 2.0 wt% of ZnF₂ and (d) Doped 3.0 wt% of ZnF₂.

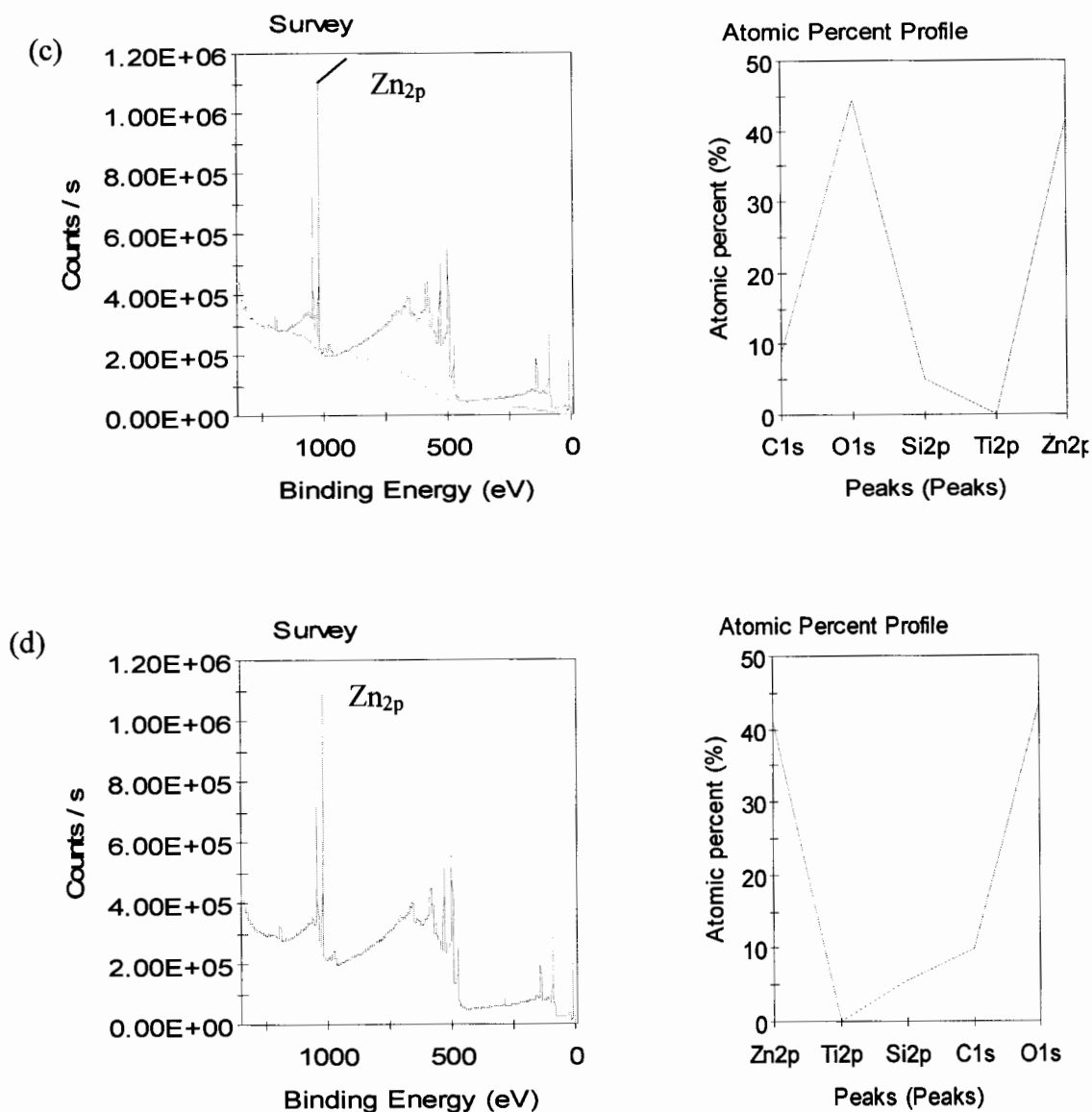


Figure 4.4 XPS spectra of ZnF₂ doped TiO₂ nanotubes with different doped ZnF₂: Undoped (b) Doped 1.0 wt%, of ZnF₂ (c) Doped 2.0 wt% of ZnF₂ and (d) Doped 3.0 wt% of ZnF₂. (continue)

X-ray photoelectron spectroscopy (XPS) was used to examine the chemical composition of the prepared samples. Figure 4.4 shows the XPS spectra of ZnF₂ doped TiO₂ nanotubes with different concentrate. Figure 4.4 displays the C_{1s}, O_{1s}, Ti_{2p}, and Zn_{2s} spectra peaks ZnF₂ doped TiO₂ nanotubes.

XPS analysis was employed to confirm the Zn doping and to explore the chemical state of the undoped and doped TiO₂ nanotubes. Fig. 4.3 shows the survey spectra of

undoped as well as doped nanotubes. XPS spectra corresponding to C_{1s}, O_{1s}, Ti_{2p}, and Zn_{2s} spectra peaks are analyzed by using XPS. For undoped TiO₂ nanotubes, the O_{1s} spectrum (Fig. 4a) shows two components, 530.7 and 532 eV, which can be assigned to the lattice oxygen in TiO₂ (Ti-O) and to the surface hydroxyl group of TiO₂ (Ti-OH), respectively [34,35]. Similarly, in Ti_{2p} peak (Fig. 4a), the spin-orbit splitting of the Ti_{2p} leads to two 2p components, located at 459.3 (Ti 2p_{3/2}) and 464.0 eV (Ti 2p_{1/2}). From these peak positions it can be concluded that the core level spectrum of Ti is of anatase phase (Ti⁴⁺) [36]. Further, Fig. 4(b-d) show the XPS spectra of Zn doped TiO₂-NTs, which reveal that the doped nanotubes are composed of three elements, that is, O 1s, C 1s, and Zn 2p. It is clear that the atomic percent profile of Zn are increased when compared to pure TiO₂.

4.5 The efficiencies of dye-sensitized solar cells

The performance of the as-prepared samples was tested in DSSCs. The current-voltage characteristics are displayed in Figure 4.5. The conversion efficiencies are shown in Table 4.1. As observed in Table 4.1, the power conversion efficiency of the doped samples decreases with increase in dopant amount. A maximum efficiency of 7.98 % was obtained for the sample undoped. At 1.0 wt%, 2.0 wt%, and 3.0 wt% of ZnF₂, the efficiency of the DSSC is found to be less than that with 7 %. This indicates that there is a limit to the amount of dopant above which the efficiency starts to decrease.

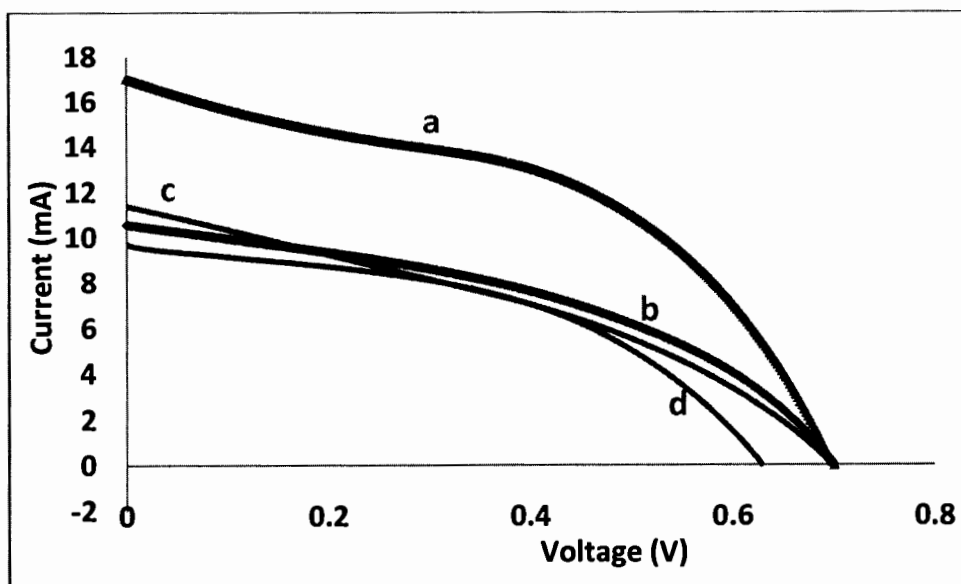


Figure 4.5 Current-Voltage curves of DSSCs with TNT doped with different amounts of ZnF_2 using ammonia as source - (a) undoped, (b) 1.0 wt%, (c) 2.0 wt%, and (d) 3.0 wt%

Table 4.1 Efficiencies of DSSCs with ZnF_2 -doped TNT with different amounts of ZnF_2

Amount of ZnF_2	V_{oc} (volts)	I_{sc} (mA/cm^2)	V_{Max} (volts)	I_{Max} (mA/cm^2)	FF	η (%)
Undoped	0.70	16.00	0.45	11.67	0.47	7.6
1.0 wt%	0.70	10.56	0.46	6.84	0.43	4.54
2.0 wt%	0.69	11.40	0.44	6.53	0.37	4.16
3.0 wt%	0.63	09.71	0.42	6.76	0.46	4.01

In efficiency for 1.0 wt%, 2.0 wt%, and 3.0 wt% of ZnF_2 could be due to optical band gap reduction as Zinc incorporates into the TNT [76]. For one, too much Zinc may cause many oxygen vacancies in the TiO_2 lattice. These vacancies would serve as recombination centers for the charge carriers (electrons and holes). As a result, there is a decrease in the conversion efficiency.

CHAPTER 5

CONCLUSION AND RECOMMENDATIONS

Titania nanotube arrays and Zn-doped titania nanotubes were fabricated by DC anodization at 50 Volts for 2 hours at room temperature in different electrolyte solutions containing different concentrations of ZnF_2 . The electrolytes were prepared by mixing ethylene glycol (EG) ammonium fluoride (0.3wt% NH_4F), de-ionized water (2Vol% H_2O) and contained different concentrations of ZnF_2 . The dopants were varied from 1.0 wt%, 2.0wt%, and 3.0 wt%, of ZnF_2 . The electrolytes were mixed by stirred at room temperature for 1 hour by a magnetic stirrer and aged at room temperature for 24 hours before being used. The as anodized samples were crystallized by annealing at 450 °C for 2 hours. From our observation, gas bubbles were observed during the anodization process. In the first step, the current density between the electrodes was very high and lower when the anodizing time was extended. The gas generation slowed down as the current density decreased. The results of the characterization, fabrication and performance tests of the DSSCs can be summarized as follows:

The influence of Zn doping on the microstructure of the nanatube film was analyzed through XRD. The structural phase of Titania nanotube arrays and Zn-doped titania nanotubes was anatase. The diffraction peaks are ascribed to TiO_2 and titanium substrate. In addition, the peaks of TiO_2 become weaker after the deposition of ZnO. The emergence of ZnO peaks and the weakening of TiO_2 peaks evidently confirm the successful growth of ZnF_2 doped TiO_2 nanotubes.

The synthesized TiO_2 nanotubes have averaged diameter of about 66 nm, wall of about 15 nm, and approximately 1.47 μm in length. When synthesized ZnF_2 doped TiO_2 nanotubes showed nanotubes wall are increase when compared to pure TiO_2 .

The XPS spectra of ZnF_2 doped TiO_2 nanotubes with different concentrate are displays the C_{1s} , O_{1s} , Ti_{2p} , and Zn_{2s} spectra peaks ZnF_2 doped TiO_2 nanotubes. XPS

analysis was employed to confirm the Zn doping and to explore the chemical state of the undoped and doped TiO₂ nanotubes. It is clear that the atomic percent profile of Zn is increased when compared to pure TiO₂.

The power conversion efficiency of the doped samples decreases with increase in dopant amount. A maximum efficiency of 4.54 % was obtained for the sample doped with 1.0 wt% of ZnF₂. This indicates that there is a critical dopant concentration, above which the efficiency starts to drop.

This work presented the study of preparation and some properties of TiO₂ and Zn-doped TiO₂ nanotube arrays film fabricated in organic electrolytes by the anodization method. For future work, it would be interesting to extend the studies of the UV-Visible properties, and test lithium ion batteries (LIBs). Remarkable have been devoted to expand the application of lithium ion batteries (LIBs) to military, aerospace, and electric vehicles, beyond the function of energy storage devices in consumer electronics, mainly due to their excellent energy density, low cost, no memory effect, and a slow loss of charge when not in use.

REFERENCES

REFERENCES

- [1] O'Regan B, Grätzel M. "A low-cost, high-efficiency solar cell based on dye sensitized colloidal TiO₂ films", **Nature**. 353: 737–739; October, 1991.
- [2] Yanyan Zhang, et al. "Synthesis and characterization of TiO₂ nanotube for humidity sensing", **Applied Surface Science**. 254(17): 5545-5547; June, 2008.
- [3] J.H. Park, S. Kim, A.J. Bard. "Novel carbon-doped TiO₂ nanotube arrays with high aspect ratios for efficient solar water splitting", **Nano Letters**. 6(1): 24-28, 2006.
- [4] R. Dholan and et al. "Hydrogen production by photocatalytic water-splitting using Cr- or Fe-doped TiO₂ composite thin films photocatalysts", **International Journal of Hydrogen Energy**. 34(13): 5337–5346; July, 2009.
- [5] N. Kilinc, E. Sennik and Z.Z. Ozturk. "Fabrication of TiO₂ nanotubes by anodization of Ti thin films for VOC sensing", **Thin Solid Films**. 520(3): 953-958; November, 2011.
- [6] E. Arpac and et al. "Photocatalytic performance of Sn-doped and undoped TiO₂ nanostructured thin films under UV and vis-lights", **Journal of Hazardous Materials**. 140(1-2): 69-74; February, 2007.
- [7] Clemens Burda, Yongbing Lou and et al. "Enhanced Nitrogen-doping in TiO₂ nanoparticles", **Nano Letters**. 3(8): 1049-1051; July, 2003.
- [8] Doohun Kim and et al. "Bamboo-type TiO₂ nanotubes: Improved Conversion Efficiency in Dye-sensitized solar cells", **J.AM.CHEM.SOC**. 130(49): 16454-16455; November, 2008.
- [9] Shiqi Li and et al. "The role of the TiO₂ nanotubes array morphologies in the dye-sensitized solar cells", **Thin Solid Films**. 520(2): 689-693; November, 2011.
- [10] Jiaqing Geng and et al. "Nitrogen-doped TiO₂ nanotubes with enhanced photocatalytic activity synthesized by a facile wet chemistry method", **Materials Research Bulletin**. 44(1): 146-150, 2009.

REFERENCES (CONTINUED)

- [11] Zuoli He and et al. "Electrochemical behavior and photocatalytic performance of Nitrogen-doped TiO₂ nanotubes arrays powders prepared by combining anodization with solvothermal process", **Ceramics International**. 39(5): 5545-5552; July, 2013.
- [12] T. Maiyalagan, B. Viswanathan and U. Varadaraju. "Fabrication and Characterization of uniform TiO₂ nanotube arrays by sol-gel template method", **Bulletin of Material Science**. 29(7): 705-708; December, 2006.
- [13] J.M. Macak, H. Tsuchiya and P. Schmuki, "High-aspect-ratio TiO₂ nanotubes by anodization of titanium", **Angew. Chem. Int. Ed.** 44(14): 2100-2102; March, 2005.
- [14] Hailei Li and et al. "Synthesis and investigation of TiO₂ nanotubes array prepared by anodization and their photocatalytic activity", **Ceramics International**. 38(7): 5791-5797; September, 2012.
- [15] Buagan Samran, P. Kronkitsiri and et al. "Preparation and microstructure of titania nanotube arrays by anodization method", **Advanced Materials Research**. 802: 104-108; August, 2013.
- [16] Hee Yeon Hwang and et al. "Influence of the organic electrolyte and anodization conditions on the preparation of well-aligned TiO₂ nanotube arrays in dye-sensitized solar cells", **Solar Energy**. 85(7): 1551-1559; July, 2011.
- [17] Jiahua Ni and et al. "Preparation of near micrometer-sized TiO₂ nanotube arrays by high voltage anodization", **Materials Science and Engineering C**. 33(1): 259-264; January, 2013.
- [18] Narongsak Kodtharin, Rinnatha Vongwatthaporn, Udom Tipparach. "The Phase Transformation and Structures of Titania Nanotubes Arrays prepared by Anodization Method", **UBRU International Conference**. 4: 455-459, 2014.
- [19] Emmanuel Nyambod Timah, Buagun Samran, Udom Tipparach. "Fabrication and Characterization of TiO₂ nanotubes for Dye-Sensitized Solar Cells", **Journal of Material Science and Engineering**. 4: 61, 2015.

REFERENCES (CONTINUED)

- [20] Nana Amponsah Kyeremateng and et al. "Properties of Sn-doped TiO₂ nanotubes fabricated by anodization of co-sputtered Ti-Sn thin films", **Electrochemical Acta**. 62: 192-198; February, 2012.
- [21] Aadesh P. Singh and et al. "Iron doped nanostructured TiO₂ for photoelectrochemical generation of hydrogen", **International Journal of Hydrogen Energy**. 33(20): 5363-5368; October, 2008.
- [22] Craig A. Grimes and Gopal K. Mor. **TiO₂ nanotube arrays: Synthesis, properties and application**. New York: Springer Dordecht Heidelberg, 2009.
- [23] Yi-Chun Liao. **Preparation of TiO₂ nanotubes by anodization process and its application on photocatalytic degradation of Acid Red 4 in aqueous solution**. Master's Thesis: National Taiwan University of Science and Technology, 2011.
- [24] C. S. Chen, S. Z. Yi and C. Wang. "Effect of the pH level of the electrolyte on the photocatalytic performance of TiO₂ nanotubes", in **Advanced materials and structural engineering: Proceeding of the international conference on advanced materials and engineering structural technology (ICAMEST 2015)**. p.111–114. Qingdao China: CRC Press, 2015.
- [25] Somkuan Photharin and Udom Tipparach. "The Effect of Preparation of Electrolytes on Microstructure and Optical Properties of Ag-Doped TiO₂ Nanotubes", **Middle-East Journal of Scientific Research**. 24(2): 332–337; February, 2016.
- [26] Alain Robin and et al. "Formation of TiO₂ Nanotube Layer by Anodization of Titanium in Ethylene Glycol-H₂O Electrolyte", **Journal of Surface Engineered Materials and Advanced Technology**. 4(3): 123–130; April, 2014.

REFERENCES (CONTINUED)

- [27] Mohd Hasmizam Razali and et al. "Morphological structural and optical properties study of transition metal ions doped TiO₂ nanotubes prepared by hydrothermal method", **International journal of material, mechanics, and manufacturing**. 1(4): 314–318; November, 2013.
- [28] E. Grabowska and et al. "Boron-doped TiO₂ Characteristics and photoactivity under visible light", **Procedia Chemistry**. 1(2): 1553–1559; November, 2009.
- [29] Soon Wook Kim and et al. "Wetting and Photocatalytic Properties of TiO₂ Nanotube Arrays Prepared via Anodic", **International Journal of Photoenergy**. 2015: 1–6; September, 2015.
- [30] D. Regonini and et al. "A review of growth mechanism, structure and crystallinity of anodized TiO₂ nanotubes", **Materials Science and Engineering: R: Reports**. 74(12): 377–406; December, 2013.
- [31] Shiqi Li and at al. "Anodization fabrication of highly ordered TiO₂ nanotubes", **Journal of Physical Chemistry C**. 113(29): 12759–12765; 9 June, 2009.
- [32] M. Szkoda, K. Siuzdak and A. Lisowska-Oleksiak. "Optimization of electrochemical doping approach resulting in highly photoactive iodine-doped titania nanotubes", **Journal of Solid State Electrochemistry**. 20(2): 563–569; February, 2016.
- [33] Nadarajah Kannan and Divagar Vakeesan. "Solar energy for future world: A review", **Renewable and Sustainable Energy Reviews**. 62: 1092–1105; September, 2016.
- [34] George W. Crabtree and Nathan S. Lewis. "Solar energy conversion", **Physics Today**. 60(3): 37-42; July, 2007.
- [35] Fujishima, A., K. Hashimoto and T. Watanabe. **TiO₂ Photocatalysis Fundamentals and Application**. Tokyo: BKC, Inc., 1999.
- [36] Macák, J.M. and et al. "TiO₂ Nanotubes: Self-organized Electrochemical Formation, Properties and Applications", **Curr. Opin. Solid State Mater. Sci**. 11(1-2): 3-18; February–April, 2007.

REFERENCES (CONTINUED)

- [37] Hoyer, P. "Formation of a Titanium Dioxide Nanotube Array", **Langmuir**. 12(16): 1411-1413; March, 1996.
- [38] Kasuga, T., M. and et al. "Formation of Titanium Oxide Nanotube", **Langmuir**. 14(12): 3160-3163; May, 1998.
- [39] Ou, H. H. and S. L. Lo. "Review of Titania Nanotubes Synthesized via the Hydrothermal Treatment: Fabrication, Modification, and Application", **Separation and Purification Technology**. 58(1): 179-191; December, 2007.
- [40] Wang, Y. Q. and et al. "Microstructure and Formation Mechanism of Titanium Dioxide Nanotubes", **Chem. Phys. Lett.** 365(5-6): 427-431; November, 2002.
- [41] J.M. Macak and et al. "TiO₂ nanotubes: Self-organized electrochemical formation, properties and applications", **Current Opinion in Solid State and Materials Science**. 11(1-2): 3-18; February-April, 2007.
- [42] G.E Thompson. "Porous anodic alumina: fabrication, characterization and applications", **Thin Solid Films**. 297(1-2): 192-201; 1 April, 1997.
- [43] A. Pakes and et al. "Development of porous anodic films on 2014-T4 aluminium alloy in tetraborate electrolyte", **Corrosion Science**. 45(6): 1275-1287; June, 2003.
- [44] Andrew J. Leenheer and et al. "Fabrication of nanoporous titania on glass and transparent conducting oxide substrates by anodization of titanium films", **Journal of Materials Research**. 22(3):681-687, March, 2007.
- [45] Gopal K. Mor and et al. "A review on highly ordered, vertically oriented TiO₂ nanotube arrays: Fabrication, material properties, and solar energy applications", **Solar Energy Materials and Solar Cells**. 90(14): 2011-2075; 6 September, 2006.
- [46] Albu, S. P., D. Kim and P. Schmuki. "Growth of Aligned TiO₂ Bamboo-type Nanotubes and Highly Ordered Nanolace", **Angew. Chem. Int. Ed.** 47: 1916-1919, 2008.

REFERENCES (CONTINUED)

- [47] Liu, S. and et al. "Synthesis and Characterization of Self-Organized Oxide Nanotube Arrays Via a Facile Electrochemical Anodization", **J. Phys. Chem. C**. 112(50): 19852-19859; November, 2008 (a).
- [48] Liu, Y. and et al. "Preparation of Short, Robust and Highly Ordered TiO₂ Nanotube Arrays and Their Applications as Electrode", **Applied Catalysis B: Environmental**. 92(3-4): 326-332; November, 2009 (a).
- [49] Liu, Y. and et al. "Comparison of Photoelectrochemical Properties of TiO₂ Nanotube-Array Photoanode Prepared by Anodization in Different Electrolyte", **Environ Chem Lett**. 7(4): 363-368; December, 2009 (b).
- [50] Liu, Y. and et al. "Comparison of Photoelectrochemical Properties of TiO₂ Nanotube-Array Photoanode Prepared by Anodization in Different Electrolyte", **Environ Chem Lett**. 363-368, 2009 (b).
- [51] Kuang, D. and et al. "Application of Highly Ordered TiO₂ Nanotube Arrays in Flexible Dye-Sensitized Solar Cells", **ACS Nano**. 2(6): 1113-1116; May, 2008.
- [52] Hattori, M. and et al. "Gas Phase Photocatalytic Decomposition of Alcohols with Titanium Dioxide Nanotube Arrays in High Vacuum", **Phys. Status Solidi C**. 8(2): 549-551; February, 2011.
- [53] Prakasam, H.E. and et al. "A New Benchmark for TiO₂ Nanotube Array Growth by Anodization", **J. Phys. Chem. C**. 111(20): 7235-7241; April, 2007.
- [54] Alivov, Y., Z. Y. Fan and D. Johnstone. "Titanium Nanotubes Grown by Titanium Anodization", **J. Appl. Phys.** 106(3): 034314; June, 2009.
- [55] Macák, J.M., K. Sirotna and P. Schmuki. "Self-organized Porous Titanium Oxide Prepared in Na₂SO₄/NaF Electrolytes", **Electrochimica Acta**. 50(18): 3679-3684; June, 2005.
- [56] Wang, D. and et al. "TiO₂ Nanotubes with Tunable Morphology, Diameter, and Length: Synthesis and Photo-Electrical/Catalytic Performance", **Chem. Mater**. 21(7): 1198-1206; March, 2009.

REFERENCES (CONTINUED)

- [57] Mor, G.K. and et al. "Enhanced Photocleavage of Water Using Titania Nanotube Arrays", **Nano Lett.** 5(1): 191-195, 2005.
- [58] Sreekantan, S. and et al. "Influence of Electrolyte pH on TiO₂ Nanotube Formation by Ti Anodization", **J. Alloys Compd.** 485(1-2): 478-483; October, 2009.
- [59] Allam, N. K. and M. A. El-Sayed. "Photoelectrochemical Water Oxidation Characteristics of Anodically Fabricated TiO₂ Nanotube Arrays: Structural and Optical Properties", **J. Phys. Chem, C.** 114(27): 12024-12029, 2010.
- [60] Awitor, K.O. and et al. "Photo-Catalysis Using Titanium Dioxide Nanotube Layers" **J. Photochem. Photobiol, A.** 199(2-3): 250-254; September, 2008.
- [61] Schulte, K. L., P. A. DeSario and K. A. Gray. "Effect of Crystal Phase Composition on the Reductive and Oxidative Abilities of TiO₂ Nanotubes under UV and Visible Light", **Appl. Catal, B.** 97(3-4): 354-360; June, 2010.
- [62] Smith, Y. R., A. Kar and V. Subramanian. "Investigation of Physicochemical Parameters that Influence Photocatalytic Degradation of Methyl Orange over TiO₂ Nanotubes", **Ind. Eng. Chem, Res.** 48(23): 10268-10276, 2009.
- [63] Lai, Y. and et al. "Effects of the Structure of TiO₂ Nanotube Array on Ti Substrate on Its Photocatalytic Activity", **J. Electrochem, Soc.** 153(7): D123-D127, 2006.
- [64] Quan, X. and et al. "Photoelectrocatalytic Degradation of Pentachlorophenol in Aqueous Solution Using a TiO₂ Nanotube Film Electrode", **Environ. Pollut.** 147(2): 409-414; May, 2007.
- [65] Brugnera, M. F. and et al. "Bisphenol A Removal from Wastewater Using Self-Organized TiO₂ Nanotubular Array Electrodes", **Chemosphere.** 78(5): 569-575; January, 2010.
- [66] Wu, X. and et al. "Enhanced Photoelectrocatalytic Degradation of Methylene Blue on Smooth TiO₂ Nanotube Array and Its Impedance Analysis", **J. Electrochem, Soc.** 156(5): K65-K71, 2009.

REFERENCES (CONTINUED)

- [67] Sun, L. and et al. "Effect of Electric Field Strength on the Length of Anodized Titania Nanotube Arrays", **J. Electroanal. Chem.** 637(1-2): 6-12; December, 2009.
- [68] Lai, Y. K. and et al. "Nitrogen-Doped TiO₂ Nanotube Array Films with Enhanced Photocatalytic Activity under Various Light Sources", **J. Hazard. Mater.** 184(1-3): 855-863; December, 2010.
- [69] Liu, Y. and et al. "Highly Stable CdS-Modified Short TiO₂ Nanotube Array Electrode for Efficient Visible-Light Hydrogen Generation", **Int. J. Hydrogen Energy.** 36(1): 167-174; January, 2011.
- [70] Xie, K. and et al. "Photoelectrocatalytic Properties of Ag Nanoparticles Loaded TiO₂ Nanotube Arrays Prepared by Pulse Current Deposition.", **Electrochim. Acta.** 55(24): 7211-7218; October, 2010.
- [71] Zhang, S. and et al. "Electrodeposition Preparation of Ag Loaded N-Doped TiO₂ Nanotube Arrays with Enhanced Visible Light Photocatalytic Performance", **Catal. Commun.** 12(8): 689-693; March, 2011.
- [72] O. Carp, C.L. Huisman and A. Reller. "Photoinduced reactivity of titanium dioxide", **Progress in Solid State Chemistry.** 32(1-2): 33-177; August, 2004.
- [73] J. Nowotny, T. Bak, M.K. Nowotny, and L.R. Sheppard. "Titanium dioxide for solar-hydrogen I. Functional properties", **International Journal of Hydrogen Energy.** 32(14): 2609-2629; September, 2007.
- [74] Charles C. and et al. **Materials for energy conversion devices.** Cambridge England, New York: Woodhead Publishing Limited, 2005.
- [75] H.X. Zhu and et al. "Electronic structures and optical properties of rutile TiO₂ with different point defects from DFT + U calculations", **Physics Letters A.** 378(36): 2719-2724; July, 2014.
- [76] J. Nowotny and et al. "Solar-hydrogen: Environmentally safe fuel for the future", **International Journal of Hydrogen Energy.** 30(5) 521-544; April, 2005.

REFERENCES (CONTINUED)

- [77] Poulomi Roy, Steffen Berger and Patrik Schmuki. "TiO₂ Nanotubes: Synthesis and Applications", **Angewandte Chemie International Education**. 50(13): 2904-2939; March, 2011.
- [78] Yi Ma and et al. "Titanium Dioxide-Based Nanomaterials for Photocatalytic Fuel Generations", **Chemical Reviews**. 114(19): 9987-10043; August, 2014.
- [79] Bart Roose, Sandeep Pathak, and Ullrich Steiner. "Doping of TiO₂ for sensitized solar cells", **Chemical Society Reviews**. 44(22): 8326-8349; August, 2015.
- [80] Akihiko Kudo and et al. "Effects of doping of metal cations on morphology, activity, and visible light response of photocatalysts", **Chemical Physics**. 339(1-3): 104-110; October, 2007.
- [81] Xingxue Wang and et al. "Multi-type carbon doping of TiO₂ photocatalyst", **Chemical Physics Letters**. 444(4-6): 292-296; August, 2007.
- [82] Xiaoxing Fan and et al. "The structural, physical and photocatalytic properties of the mesoporous Cr-doped TiO₂", **Journal of Molecular Catalysis A: Chemical**. 284(1-2): 155-160; April, 2008.
- [83] E. Setiawati, and K. Kawano. "Stabilization of anatase phase in the rare earth; Eu and Sm ion doped nanoparticle TiO₂", **Journal of Alloys and Compounds**. 451(1-2): 293-296; February, 2008.
- [84] E. Gyorgy and et al. "Anatase phase TiO₂ thin films obtained by pulsed laser deposition for gas sensing applications", **Applied Surface Science**. 247(1-4): 429-433; July, 2005.
- [85] A. Orendorz and et al. "Phase transformation and particle growth in nanocrystalline anatase TiO₂ films analyzed by X-ray diffraction and Raman spectroscopy", **Surface Science**. 601(18): 4390-4394; September, 2007.
- [86] Dong Suk Kim, Shin Jung Han and Seung-Yeop Kwak. "Synthesis and photocatalytic activity of mesoporous TiO₂ with the surface area, crystallite size, and pore size", **Journal of Colloid and Interface Science**. 316(1): 85-91; December, 2007.

REFERENCES (CONTINUED)

- [87] A.R. Liu and et al. "Low-temperature preparation of nanocrystalline TiO₂ photocatalyst with a very large specific surface area", **Materials Chemistry and Physics**. 99(1): 131-134; September, 2006.
- [88] Wilasinee Kongsuebchart and et al. "Effect of crystallite size on the surface defect of nano-TiO₂ prepared via solvothermal synthesis", **Journal of Crystal Growth**. 297(1): 234-238; December, 2006.
- [89] Kyung Ho Kim and et al. "Int. J. Electrochem", **Sci**. 8: 5183-5190, 2013.
- [90] Chi-Hwan Han and et al. "Synthesis of Amorphous Er³⁺-Yb³⁺ Co-doped TiO₂ and Its Application as a Scattering Layer for Dye-sensitized Solar Cells", **Bull. Korean Chem, Soc**. 30(1): 219-223; January, 2009.
- [91] W. Choi, A. Termin, M. Hoffmann. "The Role of Metal Ion Dopants in Quantum-Sized TiO₂: Correlation between Photoreactivity and Charge Carrier Recombination Dynamics", **J. Phys. Chem**. 98(51): 13669-13679; December, 1994.
- [92] R. Asahi and et al. "Visible-light photocatalysis in nitrogen-doped titanium oxides", **Science**. 293(5528): 296-71; July, 2001.
- [93] T. Ishii, H. Kato and A. Kudo, J. "H₂ evolution from an aqueous methanol solution on SrTiO₃ photocatalysts codoped with chromium and tantalum ions under visible light irradiation", **Journal of Photochemistry and Photobiology A: Chemistry**. 163(1-2): 181-186; April, 2004.
- [94] Jie Ma and et al. "Fabrication of Ag/TiO₂ nanotube array with enhanced photocatalytic degradation of aqueous organic pollutant", **Physica E**. 58: 24-29; April, 2014.
- [95] S. Perumal and et al. "Synthesis and characterization studies of solvothermally synthesized undoped and Ag-doped TiO₂ nanoparticles using Toluene as a solvent", **International Journal of Engineering Research and Applications**. 4(7): 184-187; July, 2014.
- [96] Jun Wang and Zhiqun Lin. "Anodic formation of ordered TiO₂ nanotube arrays: Effects of electrolyte temperature and anodization potential", **Journal of Physical Chemistry C**. 113(10): 4026-4030; February, 2009.

REFERENCES (CONTINUED)

- [97] Xu Liu and et al. "Electrodeposition preparation of Ag nanoparticles loaded TiO₂ nanotube arrays with enhanced photocatalytic performance", **Applied Surface Science**. 288: 513-517; January, 2014.
- [98] Kui Zhou and et al. "Preparation and characterization of nanosilver-doped porous hydroxyapatite scaffolds", **Ceramics International**. 41(1): 1671-1676; January, 2015.
- [99] Gusev Alexander I. (2009). "nanostructured material", **Glossary of nanotechnology and related terms**. <http://eng.thesaurus.rusnano.com/wiki/article1371>. January, 2017.

CURRICULUM VITAE

NANE Rinnatha Vongwatthaporn

EDUCATION 2010-2012, Master of Science (Major in Physics)
UbonRatchathani University
UbonRatchathani, Thailand.
2002-2005, Bachelor of Science (Major in Physics)
UbonRatchathani University
UbonRatchathani, Thailand.

PUBLICATION

1. Rinnatha Vongwatthaporn¹, Narongsak Kodtharin², Udom Tipparach^{3*}, “The Synthesis and Structures of Anodize Titnia(TiO₂) Nanotubes for Energy Conversion Materials”, Advanced Materials Research Vol. 1105(2015) pp. 220-224.
2. Rinnatha Vongwatthaporn¹, Udom Tipparach^{2*}, “Synthesis and Characterization Anodized Titnia (TiO₂) Nanotubes for Enhancing Hydrogen Production”, Applied Mechanics and Materials Vol. 749 (2015) pp. 191-196.
3. E. N. Timaha, R.Vongwatthaporn, N. Kodtharin , U. Tipparach^{2*}, “Photocatalytic Performance of Fe – doped TiO₂ Nanotubes for Dye Sensitized Solar Cells”, Journal of Material Science and Applied Energy Vol. 3(2014) pp. 5-8.

CURRENT LOCATION Ubon Ratchathani
E-mail: Rinnatha.Vongwatthaporn@gmail.com

